Bachelor's Thesis

Bachelor's degree in Industrial Technology Engineering

Modelling and Control of VSC with a Photovoltaic Source

Report

Author: Ivan Serrano Subtil

Director: Marc Cheah Mañé

Announcement: 07/2021

Escola Tècnica Superior
d'Enginyeria Industrial de Barcelona

Abstract

Given the current trends in worldwide power consumption and the demand for cleaner energy sources, microgrids are an ever-growing alternative that can fulfill the desired goal of replacing fossil fuels as the primary energy source.

This study attempts to simulate the integration of photovoltaic energy and an energy storage system, which will be a battery, with the main AC grid.
Considering that both of these elements operate with Direct Current and the main grid does so in Alternative Current, some complexity will be introduced into the model and thoroughly studied to comprehend the system's behaviour properly.

Voltage Source Converters can accomplish such task, and a complex control scheme will be put in place to regulate the power flow between both sides of the converter.

Admittedly, photovoltaic energy presents a complicated structure in itself, which added to the importance of its study means that detailed research of the modelling and control of the cells composing each PV module needs to occur.
Furthermore, efficiency is paramount when implementing renewable energy sources, and thus, the maximum possible power will be extracted using MPPT algorithms.

Finally, the power flow and exchange will be thoroughly studied via simulations, which will be carried out using Matlab and Simulink software.

Contents

1 Preface **9**
- 1.1 Project origin . . . 9
- 1.2 Previous requirements . . . 9

2 Introduction **11**

3 Project objectives **13**
- 3.1 Scope of the project . . . 13

4 Description of the system **15**
- 4.1 Microgrids . . . 15
- 4.2 Voltatge Source Converters . . . 16
- 4.3 Energy storage . . . 20
- 4.4 Photovoltaic source . . . 21
  - 4.4.1 PV production in Spain . . . 24

5 Battery model **27**
- 5.1 Introduction . . . 27
- 5.2 Modelling . . . 27

6 Photovoltaic energy model **31**
- 6.1 Modelling . . . 31
  - 6.1.1 PV system modelling . . . 31

7 System Control **39**
- 7.1 Battery system control . . . 39
  - 7.1.1 PLL . . . 39
  - 7.1.2 Reference computation . . . 41
  - 7.1.3 Current loop . . . 42
- 7.2 Photovoltaic source control . . . 46
  - 7.2.1 DC Voltage loop . . . 47
  - 7.2.2 Current loop . . . 49
  - 7.2.3 MPPT algorithms for PV systems . . . 51
- 7.3 Grid power control . . . 53

8 Simulations **57**
- 8.1 Parameters . . . 58
- 8.2 Photovoltaic source results . . . 60
- 8.3 General Microgrid operation . . . 64

9 Economic analysis **71**

10 Environmental Impact **73**

11 Conclusions **75**

11.1 Future work 76

References **77**

List of Figures

1 Scheme of the system and its main components. 15
2 Number of publications on MG per year [1]. 16
3 Stand-alone MG operation. 17
4 Basic electrical circuit scheme of an IGBT. [3] 17
5 Two-level IGBT VSC representation. [4] 18
6 Two-level VSC based on IGCT. [5] 18
7 Representation of a basic CTL. [6] 19
8 Left: Voltage output of a typical 2LC. Right: Voltage output of a 2LC.[6] 19
9 Scheme of one leg of an NPC VSC. [7] 19
10 Representation of one level of a FCC multilevel VSC.[7] 20
11 Scheme of a CHB converter. [7] 20
12 Energy storage technologies depending on power density (y-axis) and energy density (x-axis). [9] 21
13 Evolution of shares of power sources by year and type. [10] 22
14 Evolution of the total PV energy generation per year worldwide. [10] . . 22
15 Share of the total PV market per world region. [11] 23
16 Top countries in PV power generation per capita. [11] 23
17 Evolution of PV systems' pricing for residential use. [12] 23
18 Share of global PV market per type of use and future forecast. [12] . . . 24
19 Yearly installed and cumulative wind power in Spain. [13] 24
20 Yearly installed and cumulative PV power in Spain. [13] 25
21 Basic model representation of a battery integrated into the main grid with a VSC. [20] 27
22 Equivalent scheme of a 2LC with a battery. [20] 27
23 Model scheme of the MG's AC side. [20] 28
24 Simplified scheme of the complete model. 31
25 PV source and VSC model equivalence. [20] 32
26 Equivalent circuit diagram of the single diode model. 32
27 Diagram of a two-diode PV cell model. [15] 32
28 I-V curve used to calculate both short-circuit currents and open-circuit voltages. 35
29 I-V, P-V curves with Ns=150,140 and Np=12 (constant). 35
30 I-V, P-V curves with Ns=150 (constant) and Np=12,15. 36
31 I-V, P-V curves with G=1000W/m^2, G=800W/m^2, G=600W/m^2. 37
32 I-V, P-V curves with T=65ºC, T=45ºC and T=25ºC. 37
33 Overall control scheme of the battery model. [20] 39
34 PLL control scheme. [20] 40
35 angular velocity of the grid (blue) and its reference (red). 41
36 Working method of the reference computation. 42
37 Scheme of the current loop control with its controllers G_{ciq} and G_{cid}. . 42

38 Control schemes of traditional controllers (left) and IMC (right). [16] . 43
39 General Simulink model containing all the control systems. 45
40 Simulation of i_q (blue) and the reference i_q^* (red). 46
41 Simulation of i_d (blue) and the reference i_d^* (red). 46
42 General control scheme for the PV source model. [20] 47
43 Voltage loop control system representation. [20] 47
44 Simulation of E_{DC} (red) and E_{DC}^* (blue). 49
45 Simulink model of the control systems involved in the PV source model. 50
46 current i_{qPV} (blue) and reference i_{qPV}^* (red). 51
47 MPPT operation scheme integrated into the MG. 52
48 General scheme of the power control. 53
49 Response of the active power (P_z) vs the reference (P_z^*). 55
50 Standardized copper wire sizing (AWG) and its maximum current. . . . 57
51 Representation of the MG's AC side with the addition of line losses. . . . 58
52 Simulink scheme integrating an AC load into the grid. 59
53 Irradiance values in Barcelona during the day. 60
54 Temperature input used for simulations in Simulink. 60
55 Evolution of the DC bus voltage. 61
56 Close up of the PV DC voltage. 62
57 Evolution of I_{qPV} current component vs its reference I_{qPV}^* 62
58 Upper graph shows the evolution of the reactive power reference. Lower graph shows I_{dPV} vs I_{dPV}^* 63
59 Evolution of the power generated by the PV system 64
60 Temperature input used for simulations in Simulink. 65
61 Resulting current for the battery i_{qb} 66
62 Evolution of the active power in the battery system 67
63 Evolution of all the currents involved 68
64 Evolution of all the active powers involved 69
65 Park transformation representation [20] 79

List of Tables

1 Parameters of the PV cell. 33
2 Parameters of the PV array used in the model 34
3 Short-circuit currents and open-circuit voltage results 35
4 Parameters for the PLL control 41
5 Parameters for the DC voltage loop control 49
6 Impedance paramaters and respective values 58
7 RD budget and breakdown 71
8 Equipment budget and breakdown 71
9 Total project budget 72

List of Acronyms

MG Microgrid

VSC Voltage Source Converter

PV Photovoltaic

DC Direct Current

AC Alternating Current

WT Wind Turbine

PLL Phase-Locked Loop

IGBT Insulated Gate Bipolar Transistor

MOSFET Metal-Oxide-Semiconductor Field-Effect Transistor

BJT Bipolar Junction Transistor

IGCT Insulated Gate Commutated Thyristors

2LC Two-Level Converter

MLC Multilevel Converters

NPC Neutral Point Clamped

FCC Flying Capacitor Converter

CHB Cascaded H-Bridge Converter

ESS Energy Storage System

HESS Hybrid Energy Storage System

MPPT Maximum Power Point Tracking

PI Proportional-Integral

IPT Instantaneous Power Theory

IMC Internal Model Control

AWG American Wire Gauges

1 Preface

1.1 Project origin

This project is born out of the author's interest in studying renewable energies and the mechanisms through which they can be implemented in everyday life. With the help of the tutor, all these inquiries can be explored and investigated.

On the other hand, the author has been familiarized with Microgrids beforehand. Diving into their research, a deeper level of knowledge can be obtained, which is one of the objectives set out to achieve.

Knowing the subject of interest, all the possible thesis projects from the department of electrical engineering were investigated. Photovoltaic energy was chosen over other renewable alternatives among all of them due to the author's interest. Microgrids were a stand-out topic, which resulted in the project at hand.

1.2 Previous requirements

This project requires expertise in the field of electrical engineering as well as some notions of electronics.

Furthermore, the author has been previously familiarized with voltage source converters and their applications, which can prove to be helpful taking into account their importance in this work.

Finally, control engineering is of the utmost importance and thus, dominating the use and design of controllers is essential. A wide array of controllers will be implemented throughout this thesis, varying in their design and methods used.

2 Introduction

As the world trends in the direction of circumventing fossil fuels as the primary energy source, renewable energy sources are taking their place. However, this does not come without challenges. The implementation of PV modules or wind turbines presents some complications that need to be addressed. This project attempts to do so, focusing on maximizing the power output of PV cells and the exchange of power between them and the main grid, which will be studied through a variety of controllers.

Overall, this project will describe the implementation of renewable energy in a MG, thoroughly detailing each step of the modelling and control of each element involved in such task.

Starting with the description of the system, section 4 will introduce all the elements and contextualize them in present-day literature as well as the historical use of some of them. Subsequently, both models utilized in the project will be explained in detail before joining them in a single and final model.
Each of these models necessitates control mechanisms to function properly, and hence, section 7 will set forth the frameworks to achieve such work.

Lastly, section 8 presents a simulation of all the previous work, characterizing the necessary parameters and graphs and figures to illustrate the results of these simulations.

3 Project objectives

There are many goals and targets to reach, studying the behaviour of MG and all its components being the main one.
To achieve this, breaking down the model is paramount. Starting with the VSC, modelling and analyzing their conduct is the main goal for this project and designing a control system that permits regulating the system as desired.

The source of power for this model will not only come from the main grid, but also from a photovoltaic source and a storage system capable of injecting power when needed. Both of this elements will be studied in-depth, the intricacies of their operation and the process through which they can be implemented in a MG model.
This means that a thorough study of PV cells will be carried out to correctly model and control their behaviour. Likewise, the same objective has been set out to accomplish with the storage system.

Finally, the power flow between all discussed elements, in conjunction with an AC load modelled to simulate a building, will be analyzed to understand the whole MG operation.

3.1 Scope of the project

As stated in the previous section, this project will focus on the modelling and control of all the elements involved in the MG. For this purpose, specific software will need to be used, which in this case will be Matlab/Simulink tools.

Both reactive and active power supplies are scrutinized, as well as the reaction of the system to sudden variation in some elements within it.

4 Description of the system

As described before, a PV energy source has been implemented into a grid, as well as a storage system consisting of a battery. All of this constitutes what is known as a microgrid. This chapter attempts to describe all the elements within it and the interactions between them. A schematic of the system can be observed in Figure 1:

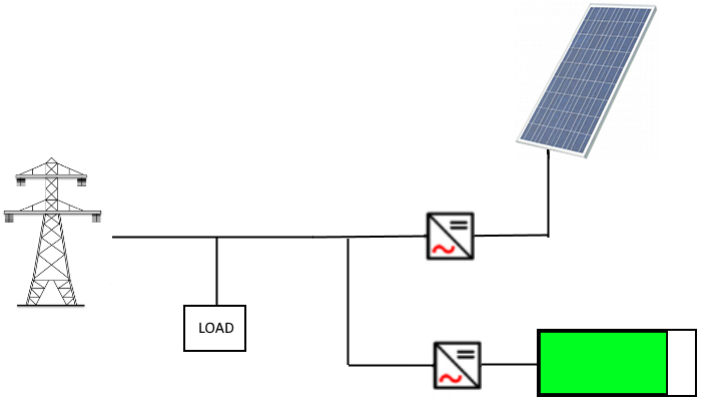

Figure 1: Scheme of the system and its main components.

Considering both the battery and the PV system operate with DC voltage and current, the use of voltage converters is needed to integrate it with an AC grid. These will exchange power between the DC and AC side, and the control system attempts to regulate this action.

These elements will connect to a three-phase AC grid using electrical cables which are not considered ideal, meaning that a resistance will be implemented in the model representing the power losses caused by parasitic resistances.

4.1 Microgrids

Microgrids are a coordinated electrical subsystem with the capability to possess multiple distributed energy resources and sustain multiple and distinct loads. Concerning their modes of operation, they can exist connected to the main grid (grid interacting MG) or, otherwise, independently as an islanded MG . Among the various advantages of their implementation, affordability and reliability stand out. Moreover, energy security can be brought to a local level, dispensing large infrastructure that is not accessible to small urban or rural areas.

Due to the aforementioned benefits and a worldwide drive to exploit renewable energy sources on the rise, the use of MG and the interest in them is rapidly increasing, as shown in Figure 2:

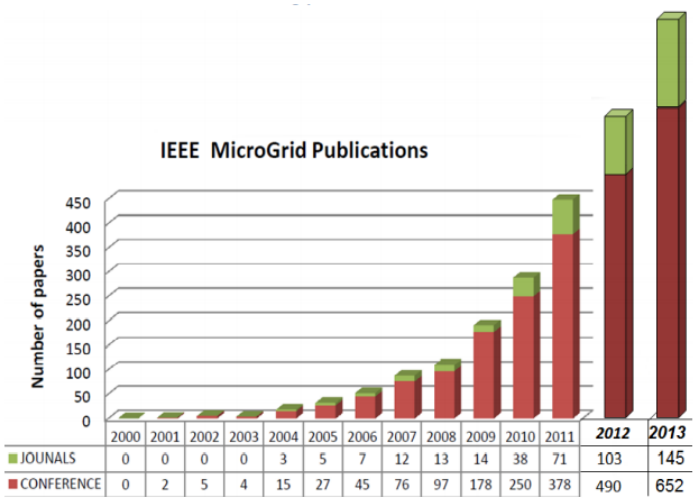

	2000	2001	2002	2003	2004	2005	2006	2007	2008	2009	2010	2011	2012	2013
JOUNALS	0	0	0	0	3	5	7	12	13	14	38	71	103	145
CONFERENCE	0	2	5	4	15	27	45	76	97	178	250	378	490	652

Figure 2: Number of publications on MG per year [1].

This phenomenon has resulted in the appearance of MGs all over the globe. One example of this can be seen in the Danish island of Samsø, home to 4000 people and capable of producing and distributing the energy required by their inhabitants and an additional 80.000 MWh of electrical energy that are fed annually back to the main grid in Denmark.
All of this has been achieved by installing a total of 21 WT (both inland and off-shore) in conjunction with PV arrays, although the latter contributes far less than the former. The on-shore WT alone is estimated to produce 28.000 MWh, equivalent to 2,1 million litres of oil [1].
The cost of this investment is calculated to be approximately 49,5 million € originating mainly from private investors, many of whom are inhabitants of the island with a strong desire for self-sustainability.

Many more examples are present all around the world, with various forms of operation and capabilities. For instance, while storage systems in the form of batteries are widely used, some public institutions reward feeding energy to the main grid, as is the case of the state of Utah, USA, where 90-92,5 per cent of that energy is monetarily compensated according to retail rates[2].

4.2 Voltatge Source Converters

VSCs are power electronic devices with multiple functionalities. For the purposes of this project, enabling the power flow between the DC and AC side of the MG is the main reason for their use.

As previously mentioned, VSCs can operate in two main modes: connected to the main grid or as stand-alone systems.
For the former, a tracking system for the grid's frequency needs to be implemented known as a phase lock loop (PLL), which will be thoroughly explained in subsection

7.1.1.

On the other hand, there is no grid-connected to the VSC in islanded MGs, which poses various challenges: excess energy produced cannot be transmitted to the main grid. Consequently, storage systems need to be implemented in order to optimize the power transfer on the MG.

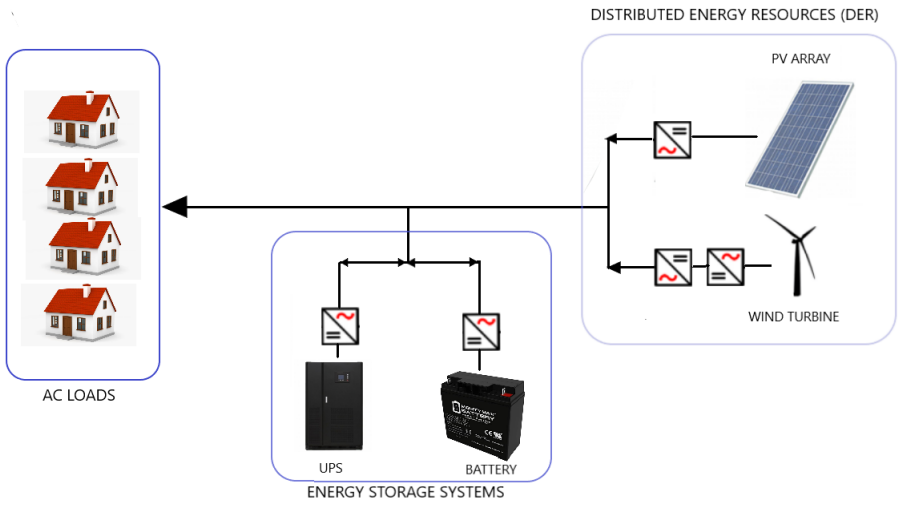

Figure 3: Stand-alone MG operation.

However, the most widely used method of classifying VSCs is regarding its type of semiconductor component:

- Insulated Gate Bipolar Transistors (IGBT) are power switching devices with characteristics from both MOSFETs and BJTs, which is reflected in their equivalent circuit modelling (Figure 4).

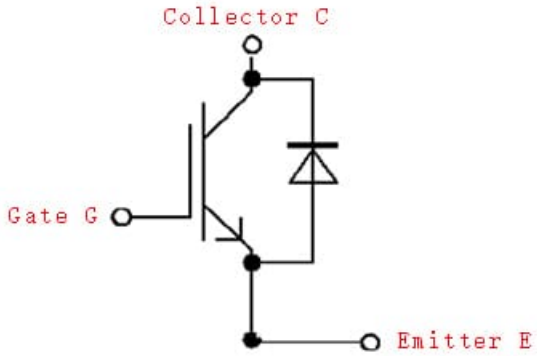

Figure 4: Basic electrical circuit scheme of an IGBT. [3]

These voltage-controlled instruments present as their main advantages fast switching times and simplicity in their implementation.
On the other hand, IGBTs are asymmetrical and, therefore, can't be used in current source converters. The typical topology for IGBT-based VSCs are as follows:

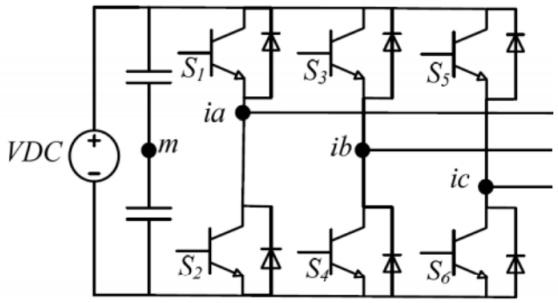

Figure 5: Two-level IGBT VSC representation. [4]

- Insulated Gate Commutated Thyristors (IGCT) fulfil the same purpose as IGBT, although differing in their features. ICGTs behave like most transistors in terms of switching but offer the benefits of low-conduction losses of thyristors, which coupled with almost negligible turn-on losses enable their use at higher frequencies than any transistor-based semiconductor, operating at frequencies up to 5KHz [5]. Furthermore, the drawbacks present in IGBTs when it comes to asymmetry are corrected for in IGCTs.

  Due to simplicity and the current state of the literature, IGBTs are more prevalent, which are the ones studied in this project.
  Nevertheless, to illustrate the differences between the two semiconductors explored, an analogue representation of the model is shown in Figure 6:

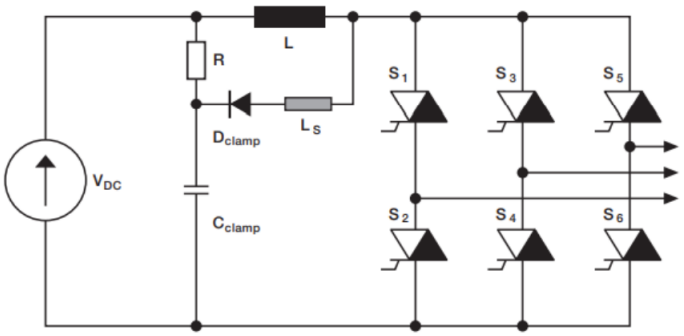

Figure 6: Two-level VSC based on IGCT. [5]

VSCs can also be categorized depending on the technology used:

- 2-level VSCs (2LC) are the earliest technology in the field, comprised of high-voltage switches that result in more significant conduction losses. Regardless,

they are proven and trustworthy, as well as of relative simplicity in their implementation. One variant that needs highlighting is two-level cascaded converters (CTL), consisting of multiple smaller two-level building blocks (Figure 7).

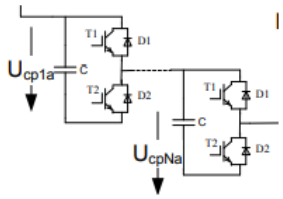

Figure 7: Representation of a basic CTL. [6]

The resulting voltage output is a sinusoidal-like waveform from the converter, instead of the usual behaviour seen in conventional 2LCs (Figure 8):

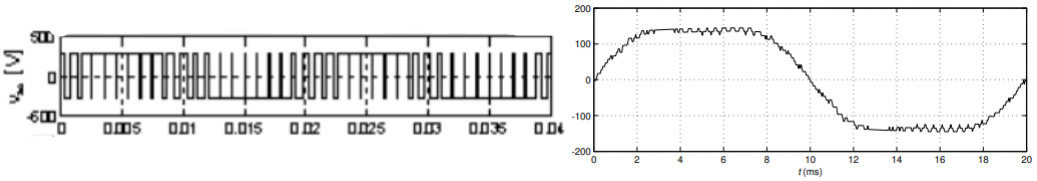

Figure 8: Left: Voltage output of a typical 2LC. Right: Voltage output of a 2LC.[6]

- Multilevel converters (MLC) reproduce these sinusoidal waveforms with a higher fidelity since they are formed by more than two voltage levels. Moreover, they allow for the use of low voltage switches resulting in lower conduction losses stemming from low switching frequencies, which added to smaller voltage drops (dv/dt) reduce the stress in cables and other components.
  - Multiple variations of MLC exist, neutral point clamped (NPC) being the most widespread in the field and the first MLC proposed. The multiple voltage levels are produced by adding capacitors in series, which difficult the overall utilization of NPC converters and, thus, only 3-level converters are commercially available [7](Figure 9).

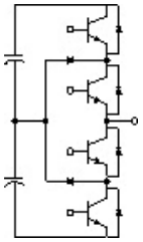

Figure 9: Scheme of one leg of an NPC VSC. [7]

– Flying capacitor converters (FCC) present highly complex DC bus structures because each one requires its own supply. Theoretically, FCC should show infinite voltage level while in reality only six levels can be seen [8](Figure 10).

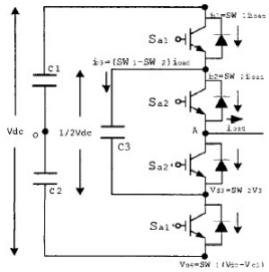

Figure 10: Representation of one level of a FCC multilevel VSC.[7]

– Lastly, Cascaded H-Bridge Converters (CHB) are similar in structure to FCCs and possess the same complexities.

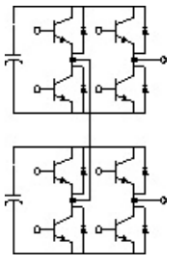

Figure 11: Scheme of a CHB converter. [7]

Overall, prioritizing simplicity in the study of converters, the technology used is that of a 2LC, which is also the most cost-friendly option of all.

4.3 Energy storage

Energy storage systems introduce many advantages, mainly when it comes to balancing power generation and demand. When implemented alongside a PV source, ESS can set aside the excess energy produced by the renewable energy source and supply it in case of a shortage of power relative to demand.
As mentioned before, ESS can be sometimes dispensable considering that some main grids can act as one, returning the energy supplied to them or at least a significant percentage of it.

There is a wide array of ESS technologies available in the market, which can be classified depending on their power and energy density (Figure 12):

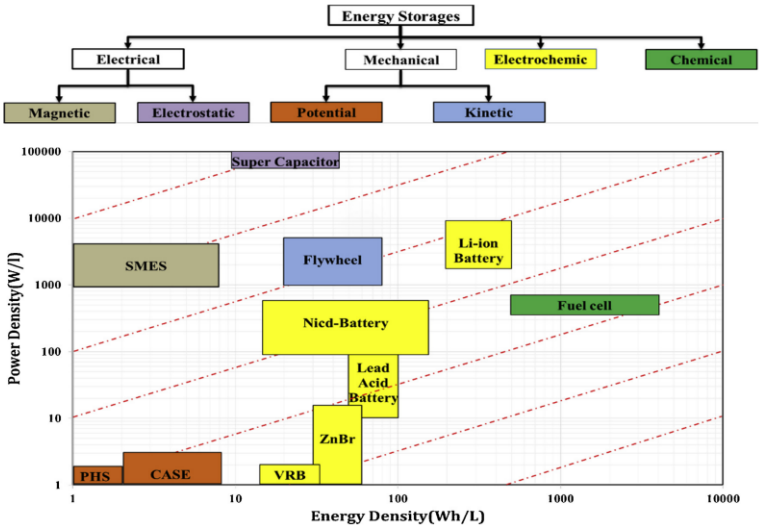

Figure 12: Energy storage technologies depending on power density (y-axis) and energy density (x-axis). [9]

Some of the problems seen in any of these technologies, such as intermittency, instability and unbalanced loads, can be corrected by merging some of them in what is known as hybrid energy storage systems (HESS). Additionally, efficiency, cost and system lifespan can be significantly improved by HESS [9].
Concerning the project at hand, further research can be made to implement a HESS to alleviate the problems associated with fluctuating power production sources such as PV systems like the one studied here.

4.4 Photovoltaic source

PV energy systems work by transforming the power irradiated by the sun into electricity. Being the most popular renewable energy, it has ranked either first or second in the last eight years among all new additions to the grid, making up 43 per cent of that share in 2020 [10](Figure 13).

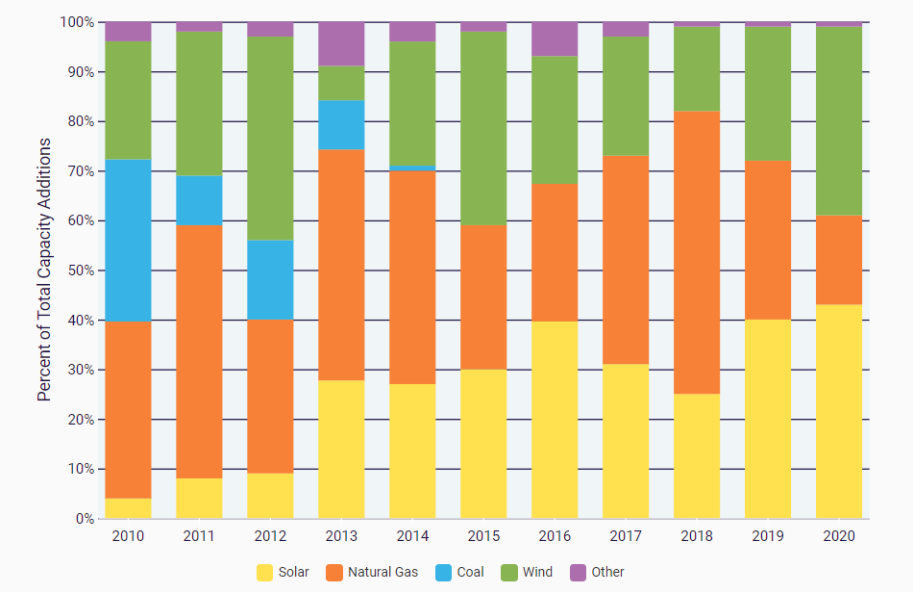

Figure 13: Evolution of shares of power sources by year and type. [10]

Cumulatively, the world has seen a rapid increase in total capacity, which can be seen in Figure 14:

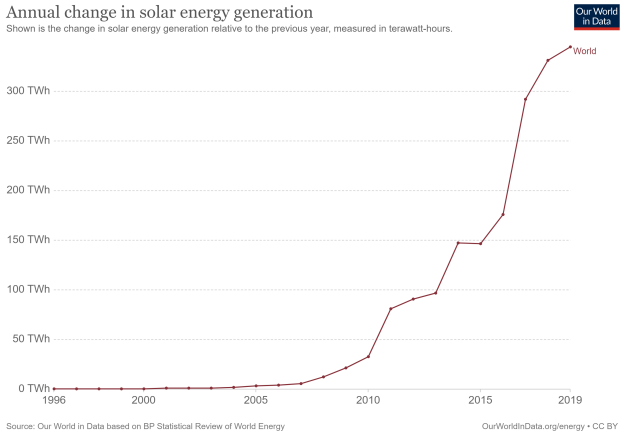

Figure 14: Evolution of the total PV energy generation per year worldwide. [10]

Per region, Asia-Pacific overwhelmingly possesses the highest capacity of PV production in the world, with China ranking first in total PV energy capacity. Factors such as population need to be taken into account, so a per capita metric is much more relevant when discussing how countries rank in PV production. According to Figure 16, countries like Germany and Australia fare more positively while China falls out of the top ranking [11](Figures 15 and 16).

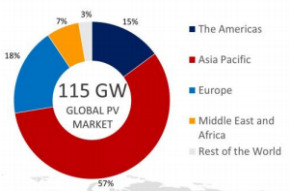

Figure 15: Share of the total PV market per world region. [11]

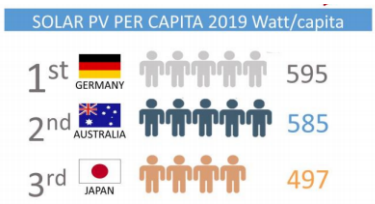

Figure 16: Top countries in PV power generation per capita. [11]

Another positive note is the decrease in PV production pricing for residential purposes, as installation costs have been steadily declining recently [pricing]. Further legislation and programs need to be implemented towards reducing barriers, facilitating and incentivizing the installation of PV systems at scale.
Residential use is still the lesser-used type among all applications, presenting the most future potential [12].

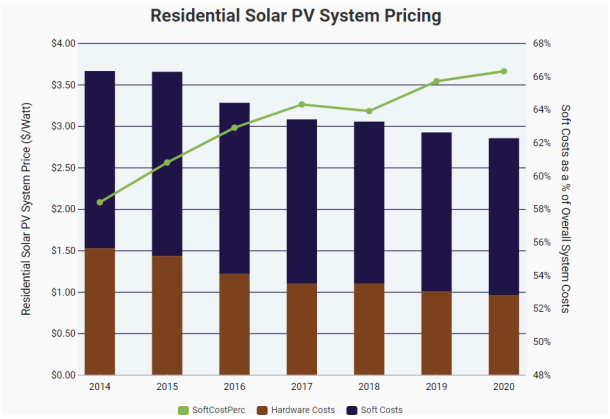

Figure 17: Evolution of PV systems' pricing for residential use. [12]

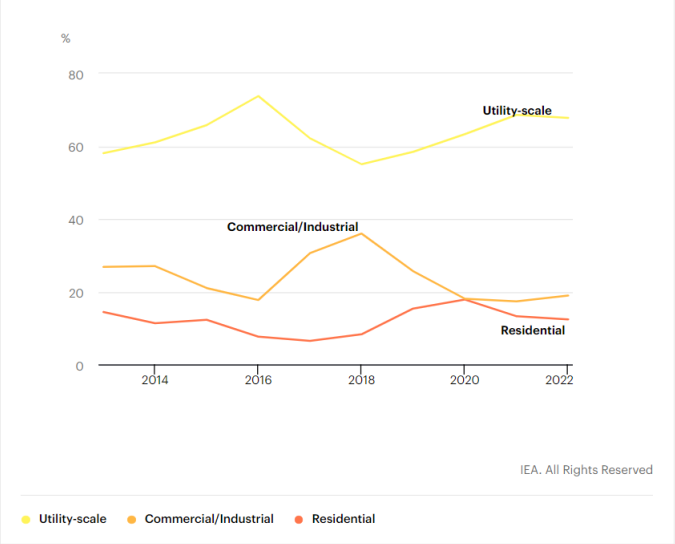

Figure 18: Share of global PV market per type of use and future forecast. [12]

4.4.1 PV production in Spain

Spain has historically been a stronghold for renewable energy production, focusing on wind and solar energy. In fact, it ranks fifth and eighth respectively globally in terms of installed capacity, 23.047 MW for wind power and 4.675 MW for solar [spain]. However, growth has decelerated since 2008, and since then, newly installed wind and solar capacity has not reached that peak again [13] (Figures 19 and 20):

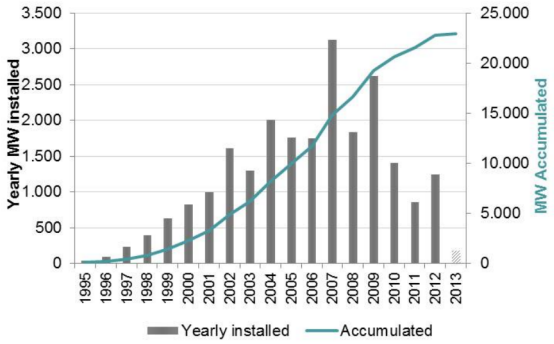

Figure 19: Yearly installed and cumulative wind power in Spain. [13]

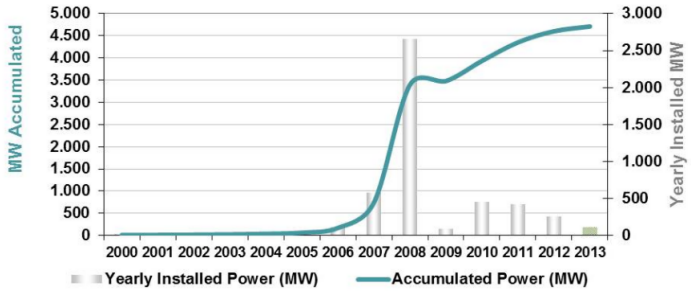

Figure 20: Yearly installed and cumulative PV power in Spain. [13]

Overall, the Iberian country continues to develop renewable energy production, which has resulted in some interesting cases like the island of El Hierro, where all the energy produced comes from renewable sources. This being one example of how Spain is pioneering alongside others the global charge towards self-sustainability.
Furthermore, the obstacle that the so-called sun tax was posing on the country's growth in PV capacity came to an end in 2018, when the government terminated the fatal legislation.

.

5 Battery model

5.1 Introduction

In this section a system with a battery connected to the main grid via a VSC will be described (Figure 21).

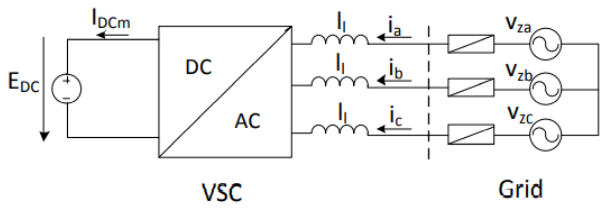

Figure 21: Basic model representation of a battery integrated into the main grid with a VSC. [20]

As observed in the figure above, the battery has been modelled as a DC voltage source, while the grid is an AC voltage source and an impedance. In between the VSC and the main grid an inductance acts as filter, smoothening the connection across both components.

5.2 Modelling

Starting with the VSC, these are comprised of 6 IGBT, which translate to an AC 3-phase voltage source on the AC side, connecting to the main grid.
Conversely, the 2LC is simplified into a DC source on the battery (or DC) side and a voltage source from the AC side (Figure 22).

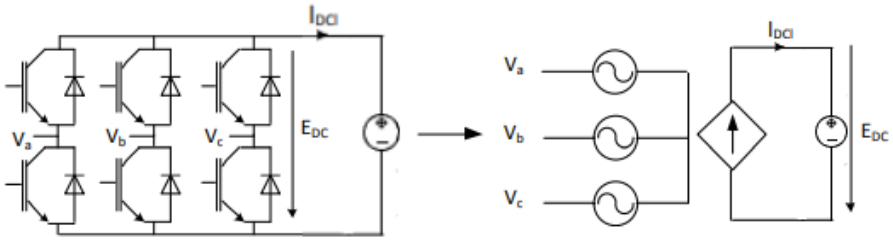

Figure 22: Equivalent scheme of a 2LC with a battery. [20]

All of the simplified elements will be controlled, and the process to do so will be described in later sections.

Both sides will be linked through an exchange of active power, ensuring a balance between DC and AC sides:

$$P_{AC} = P_{DC} \tag{5.1}$$

Thus, the current flowing through the DC side can be calculated:

$$I_{DCl} = \frac{P_{AC}}{E_{DC}} \tag{5.2}$$

Concentrating on the AC side, the corresponding scheme with the grid and VSC voltages can be seen in Figure, along with the equivalent resistance (r_l) and inductance (l_l) in:

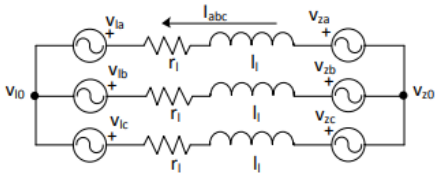

Figure 23: Model scheme of the MG's AC side. [20]

The impedance mentioned avoids connecting two sources of the same type, which can lead to short-circuits.

Following Figure 23, the voltage equation can be computed:

$$\begin{bmatrix} v_{za} \\ v_{zb} \\ v_{zc} \end{bmatrix} - \begin{bmatrix} v_{la} \\ v_{lb} \\ v_{lc} \end{bmatrix} - (v_{0l} - v_{0z}) \begin{bmatrix} 1 \\ 1 \\ 1 \end{bmatrix} = \begin{bmatrix} r_l & 0 & 0 \\ 0 & r_l & 0 \\ 0 & 0 & r_l \end{bmatrix} \begin{bmatrix} i_a \\ i_b \\ i_c \end{bmatrix} + \begin{bmatrix} l_l & 0 & 0 \\ 0 & l_l & 0 \\ 0 & 0 & l_l \end{bmatrix} + \frac{d}{dt} \begin{bmatrix} i_a \\ i_b \\ i_c \end{bmatrix} \tag{5.3}$$

Where v_{za}, v_{zb}, v_{zc} are the three-phase grid voltages, v_{la}, v_{lb}, v_{lc} are the three-phase converter voltages and i_a, i_b, i_c are the currents flowing through the model in the abc frame.

In the case of absence of a neutral conductor, the equation can be simplified into:

$$v_{l0} - v_{z0} = \frac{1}{3}[111] \cdot (v_z^{abc} - v_l^{abc}) \tag{5.4}$$

For neutrally balanced systems $v_{l0} - v_{z0} = 0$, which in conjunction with the application of the Park transformation, necessary for control, produces the following equation:

$$\begin{bmatrix} v_{zq} \\ v_{zd} \end{bmatrix} - \begin{bmatrix} v_{lq} \\ v_{ld} \end{bmatrix} = \begin{bmatrix} r_l & l_l\omega_e \\ -l_l\omega_e & r_l \end{bmatrix} \begin{bmatrix} i_q \\ i_d \end{bmatrix} + \begin{bmatrix} l_l & 0 \\ 0 & l_l \end{bmatrix} + \frac{d}{dt} \begin{bmatrix} i_q \\ i_d \end{bmatrix} \tag{5.5}$$

Where v_q, v_d, i_q, i_d are the grid voltages and currents in the qd0 reference frame and ω_e is the electrical angular velocity.

6 Photovoltaic energy model

The present chapter intends to describe the implementation of a PV energy source into the system detailed in the previous chapter (5). As is the case with a battery, a PV system requires a VSC in order to connect this DC source to the AC grid. This process needs to be mathematically expressed and modelled in order to be able to analyze and control the overall system.

6.1 Modelling

In the same way that the AC side of the VSC, linked to the DC battery, was coupled with an LC impedance, the PV source will need an equivalent impedance to avoid the connection of sources of the same type.
On the other hand, the PV array used can be modelled similarly as the battery, with the addition of a shunt capacitor to go along with a controlled DC source.

All the elements just mentioned can be combined to form the following complete model, seen in Figure 24:

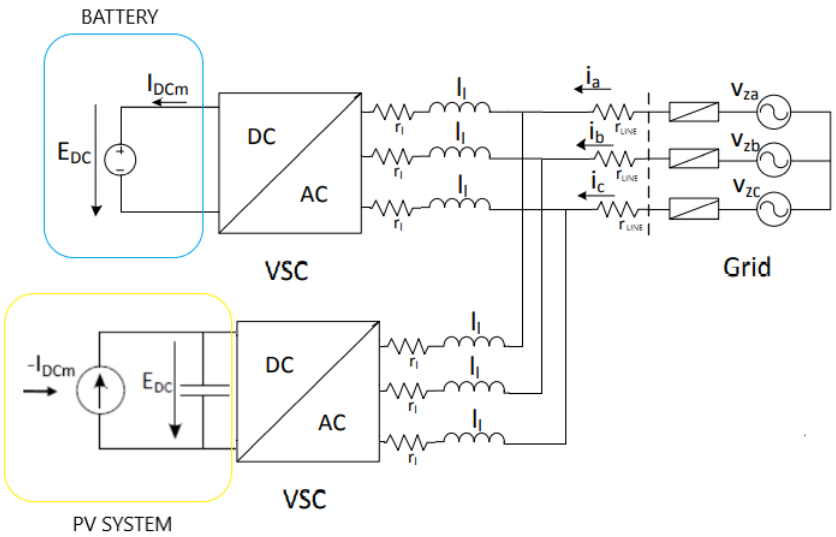

Figure 24: Simplified scheme of the complete model.

The DC capacitor, element connecting the DC side of the VSC and the PV array, integrates a shunt capacitor to ensure a power balance and keep the voltage constant of the DC bus mentioned above.

6.1.1 PV system modelling

As seen in Figure 25, the PV array's output can be modelled as a controlled current source.

Due to the variation of irradiance and temperature that occurs naturally, this current source will be a non-constant value named I_{dcm}.

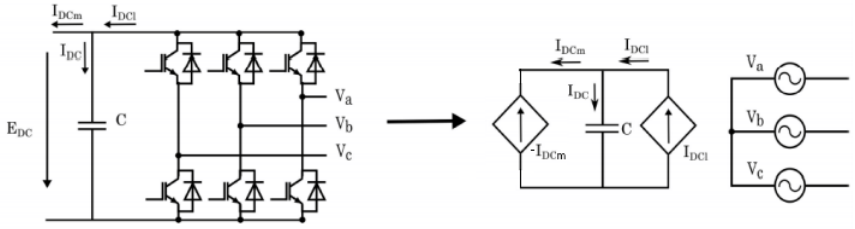

Figure 25: PV source and VSC model equivalence. [20]

The next step in studying the renewable energy source system is the modelling of a PV cell.
The single-diode model will be used for this purpose. A circuit diagram of this model can be observed in Figure 26:

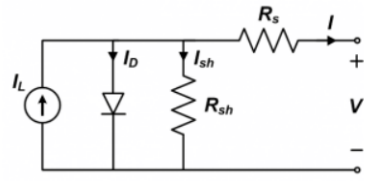

Figure 26: Equivalent circuit diagram of the single diode model.

The elements of this model are a diode, a current source and 2 resistances, one in parallel with the current source and the other in series. This model's current output is directly proportional to the light the solar cell receives
Nevertheless, the essential variable of the study is the current-voltage diagram of the cell, determined by the diode.

Other parameters were implemented in this model, which adds to its complexity, although it is not complete. Much more thorough studies have made use of a two-diode model, presented by Gow and Manning, to increase the accuracy of its characteristics [15]. The analogue representation as the one in Figure 27 being as follows:

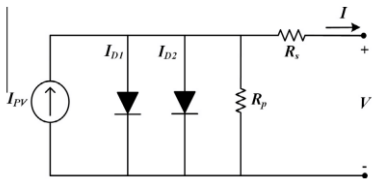

Figure 27: Diagram of a two-diode PV cell model. [15]

The previously mentioned I-V curve is described through a series of equations, with a multitude of factors that are dependant on the characteristics of the PV module used.

There are a plethora of brands and models from which to choose from, but the one studied will be the Tesla SR25T3 PV module, due to availability and brand recognition. The parameters of said module can be seen in the following table:

cells per module	6
Voltage at maximum power V_{mp}	3,5 (V)
Open circuit voltage V_{oc}	4,3 (V)
Short-circuit current I_{sc}	7,7 (A)
V_{oc} Temperature coefficient	-0,2907 (%/ºC)
I_{sc} Temperature coefficient	0,022 (%/ºC)
Maximum power	25,2 (W)

Table 1: Parameters of the PV cell.

With all the module's parameters specified, the equations describing the PV cell's model and its I-V curve can now be expressed:

$$I = I_L - I_o \cdot (\exp\frac{q(V + IR_s)}{nKT} - 1) - \frac{V + IR_s}{R_s h} \tag{6.1}$$

$$I_L = G\frac{I_{sc(T1)}}{G_o} \cdot (1 + K_o(T - T_1) \tag{6.2}$$

$$I_0 = I_{d0}(\frac{T}{T_1})^{\frac{3}{n}} \cdot \exp(-\frac{qV_g}{nK}(\frac{1}{T} - \frac{1}{T_1})) \tag{6.3}$$

$$K_0 = \frac{I_{sc(T2)} - I_{sc(T1)}}{T_2 - T_1} \tag{6.4}$$

$$I_{d0} = \frac{I_{sc(T1)}}{\exp(\frac{qV_{oc(T1)}}{nKT_1} - 1)} \tag{6.5}$$

where:
$T_1 = temperature\ 1\ (K)$
$T_2 = temperature\ 2\ (K)$
$G = irradiance\ (W/m^2)$
$I = cell\ current\ (A)$

$I_L = photo\ current\ (A)$
$I_0 = diode\ saturation\ current\ (A)$
$q = charge\ of\ an\ electron\ (C)$
$V = cell\ voltage\ (V)$
$K = Boltzmann's\ constant\ (m^2kg/s^2K)$
$R_s = series\ resistance\ (\Omega)$
$R_{sh} = shunt\ resistance\ (\Omega)$
$n = diode\ ideality\ factor$
$T = cell\ temperature\ (K)$
$V_g = band\ gap\ voltage\ (eV)$
$I_{sc(T1)} = short-circuit\ current\ at\ T_1\ (A)$
$I_{sc(T2)} = short-circuit\ current\ at\ T_2\ (A)$
$V_{oc(T1)} = open-circuit\ voltage\ at\ T_1\ (V)$

The last thing to consider before being able to simulate this model of a PV array is the model parameters, which are indicated in this table:

Number of modules per string in series N_s	190
Number of strings in parallel N_p	12
R_s	0,043068 Ω
R_{sh}	20,818 Ω
Diode ideality factor	1,04 (V)
T_1	25 (ºC)
T_2	45 (ºC)
K	$1{,}38{\cdot}10^{-23}$ (m^2kg/s^2K)
q	$1{,}6{\cdot}10^{-19}$ (C)
V_g	1,1 (eV)

Table 2: Parameters of the PV array used in the model

The parameters left to compute: $I_{sc(T1)}$, $I_{sc(T2)}$ and $V_{oc(T1)}$ need to be deduced from the I-V curves at T_1 and T_2 by looking at the axis cutting points. Subsequently, by dividing N_s for the short-circuit currents and N_p for open-circuit voltages, the final values can be obtained.
The reason for this final operation is a simple circuit-theory effect: in the case of a series connection, the short-circuit current remains constant while the open-circuit voltage is directly proportional. Conversely, in the case of a parallel connection, the current is proportional while the voltage is constant.

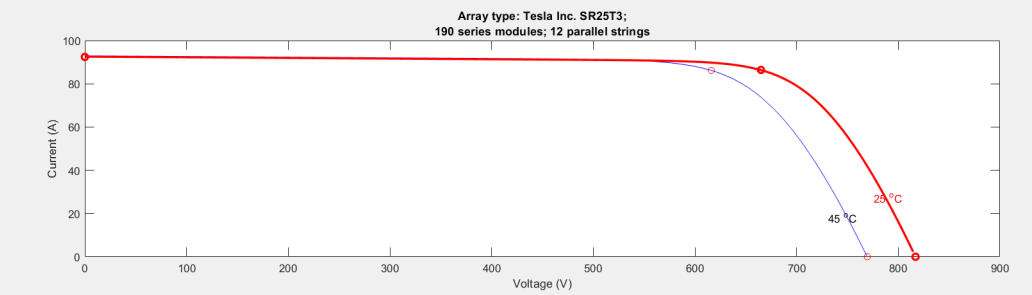

Figure 28: I-V curve used to calculate both short-circuit currents and open-circuit voltages.

$I_{sc(T1)}$	7,7 (A)
$I_{sc(T2)}$	7,735 (A)
$V_{oc(T1)}$	4,3 (V)

Table 3: Short-circuit currents and open-circuit voltage results

Some simulations can be carried out to validate the effect Ns and Np have on the I-V curve, as well as the power-voltage curve (P-V).

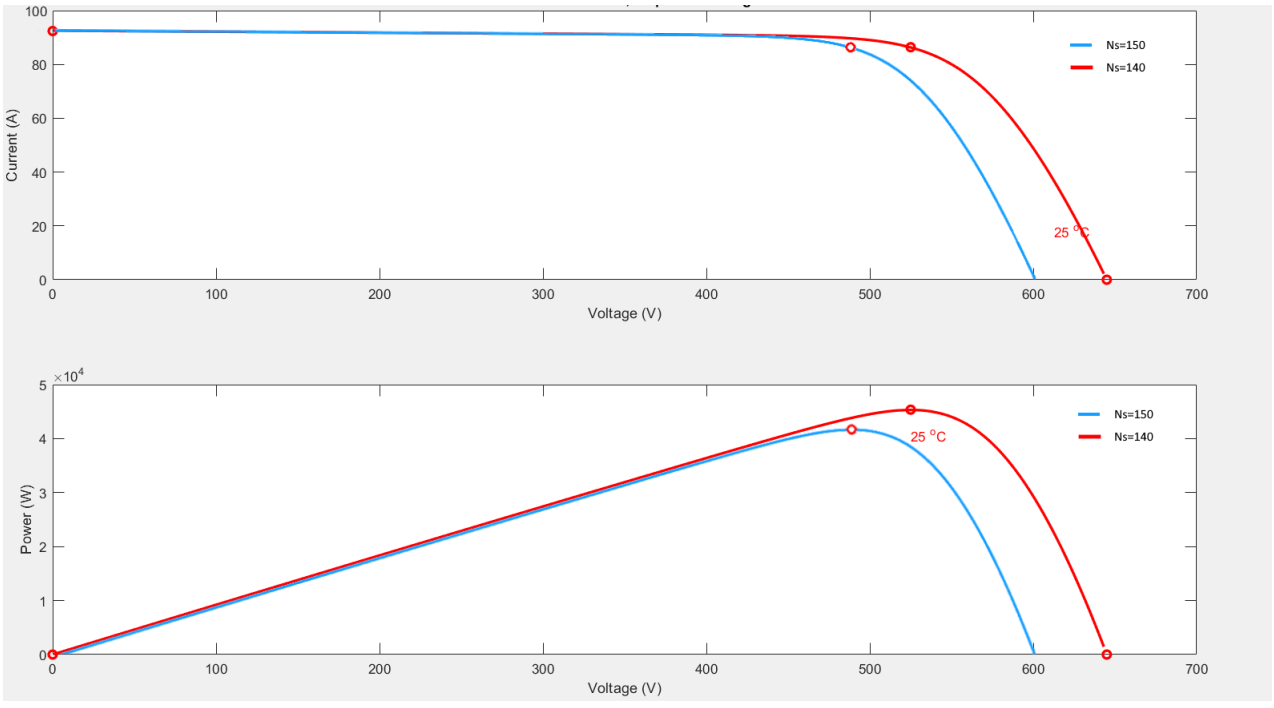

Figure 29: I-V, P-V curves with Ns=150,140 and Np=12 (constant).

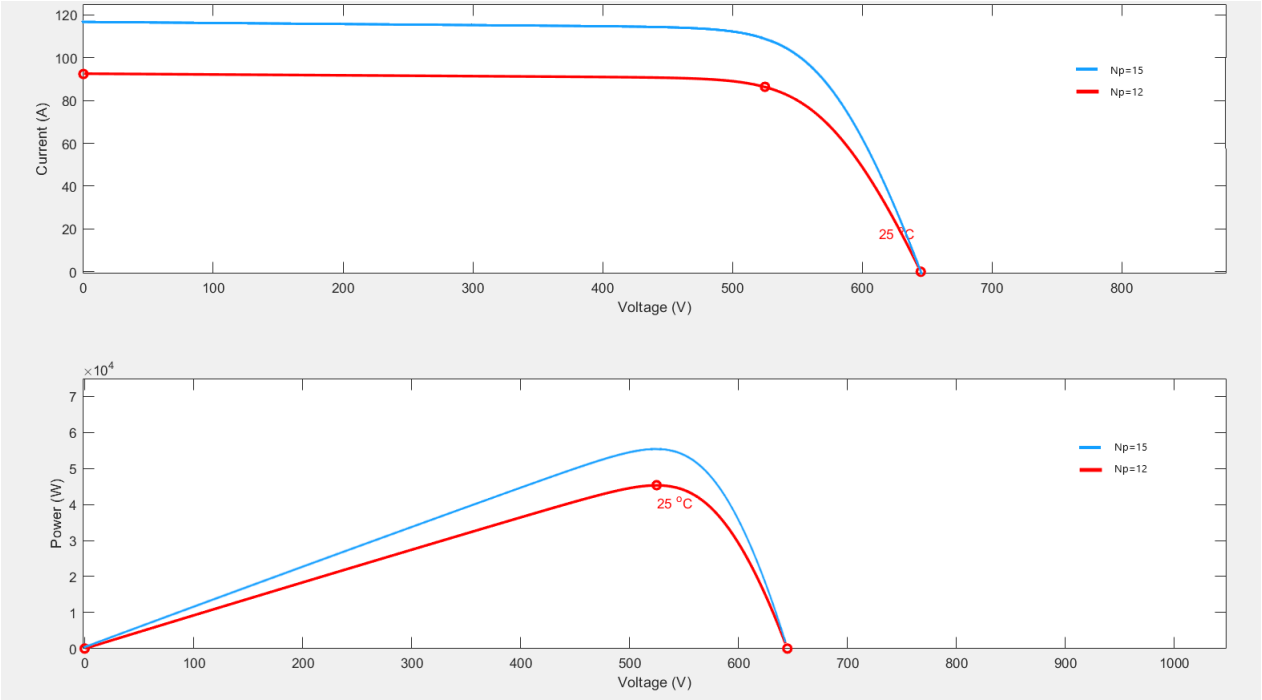

Figure 30: I-V, P-V curves with Ns=150 (constant) and Np=12,15.

As seen in Figures 29 and 30, both V_{oc} and P_{max} are directly proportional to Ns while I_{sc} remains constant . Likewise, I_{sc} and P_{max} are proportional to Np whilst not affecting V_{oc}.

Other simulations have been conducted to test the effect irradiance and temperature have on both characteristic curves:

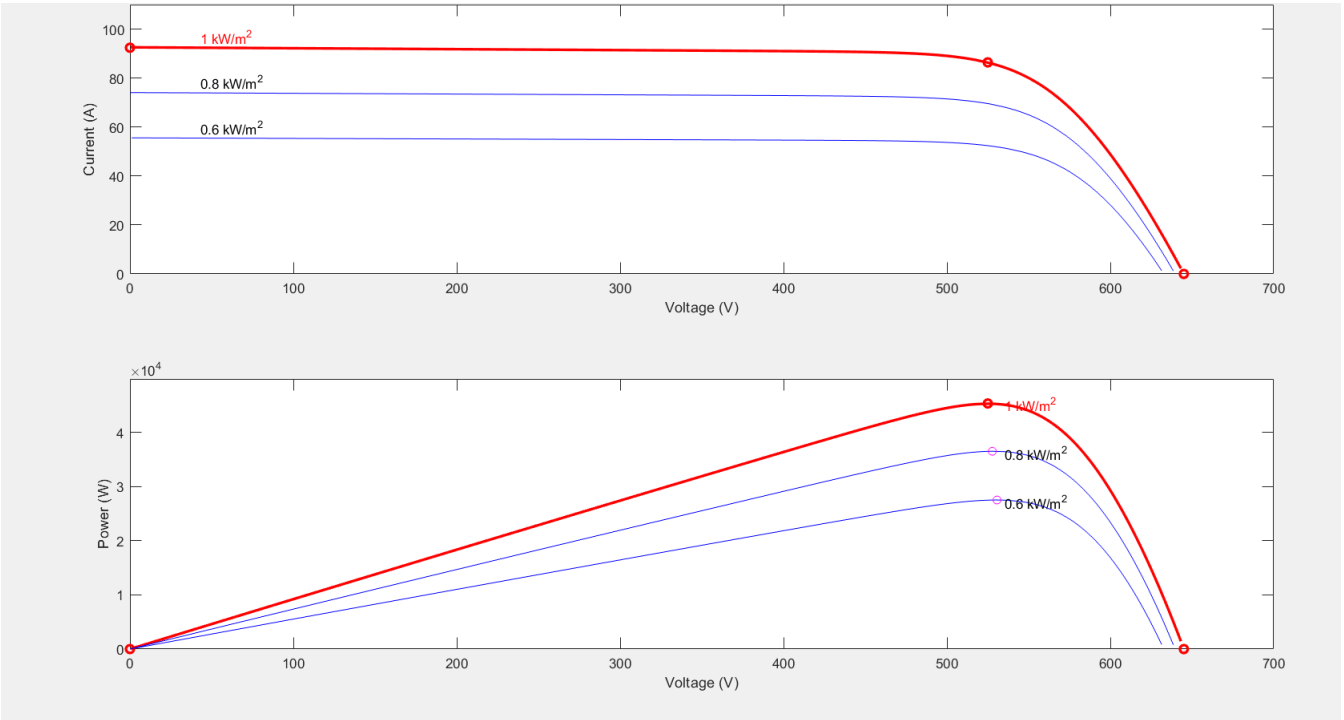

Figure 31: I-V, P-V curves with G=1000W/m^2, G=800W/m^2, G=600W/m^2.

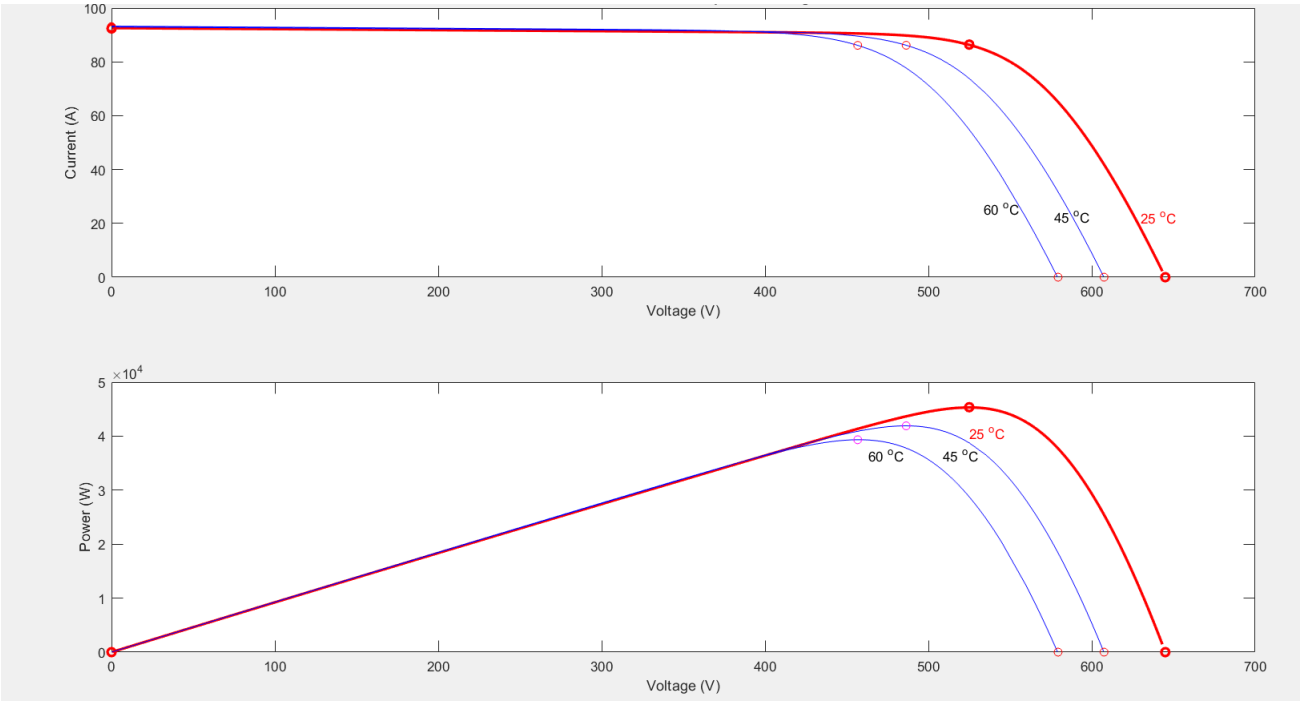

Figure 32: I-V, P-V curves with T=65ºC, T=45ºC and T=25ºC.

7 System Control

In this chapter, an effort will be made towards explaining the control methods used in order to reach the desired performance characteristics.
There are many elements to consider in this endeavour, starting with controlling the VSC's behaviour. The PV system will also need a control system in algorithm called Maximum Power Point Tracking (MPPT).

7.1 Battery system control

The control loop for this system regulates the AC in the qd0 reference frame. Before this, a phase-locked loop must be implemented to track the electrical angle.
The general control scheme used for this model can be seen in Figure 33:

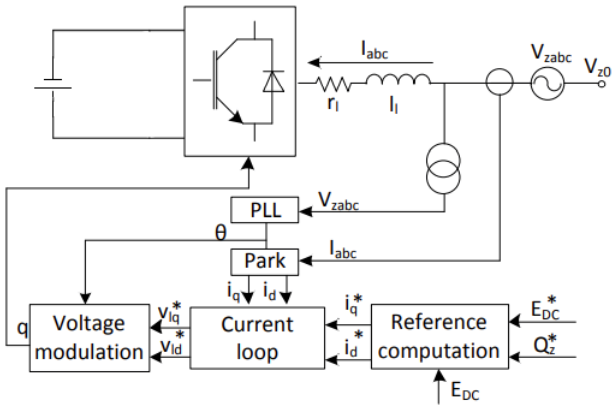

Figure 33: Overall control scheme of the battery model. [20]

7.1.1 PLL

The design of the PLL will be made according to Chung [18], whose work determined a process through which the control parameters can be deduced depending on the specifications chosen.

The loop consists of a d-axis voltage feedback with a PI controller, the output of which is the angular velocity of the grid. However, being that the desired parameter of study is the grid angle, an integrating element must be introduced:

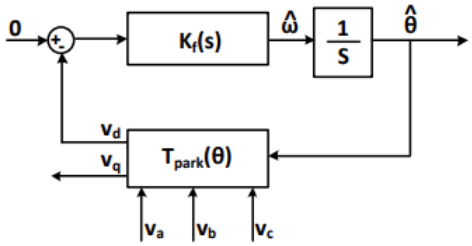

Figure 34: PLL control scheme. [20]

The PI controller used in this section can be designed starting by linearizing the system, which yields a second-order equation in the Laplace domain:

$$\frac{\hat{\theta}(s)}{\theta(s)} = \frac{2\xi\omega_e s+\omega_e^2}{s^2+2\xi\omega_e+\omega_e^2} \tag{7.1}$$

where:

$\hat{\theta}$ = estimated grid angle
θ = real grid angle
ω_e = electrical grid angular velocity
ξ = damping ratio

The controller K_f is calculated as:

$$K_f = K_p + \frac{K_p}{\tau_{PLL} s} \tag{7.2}$$

where:

τ_{PLL} = PLL's time constant
K_p = proportional constant

Comparing both equations yields a system of equations from which the control parameters can be deduced:

$$K_p = \frac{\omega_e^2 \tau_{PLL}}{E_m} \tag{7.3}$$

$$\tau_{PLL} = \frac{4\xi^2}{K_p E_m} \tag{7.4}$$

where: E_m = peak voltage value

The following table contains all the values mentioned above, which will be used for future testing:

ω_e	$2\pi 50\ (rad/s)$
ξ	$\sqrt{2}/2$
E_m	$400\sqrt{2}/\sqrt{3}\ (V)$
K_p	1,36
τ_{PLL}	0,0045

Table 4: Parameters for the PLL control

Some simulations have been carried out with Matlab/Simulink to validate the model. The following plot, Figure 35, shows the behaviour of the grid's angular velocity against the reference ω_e, verifying the controller's design:

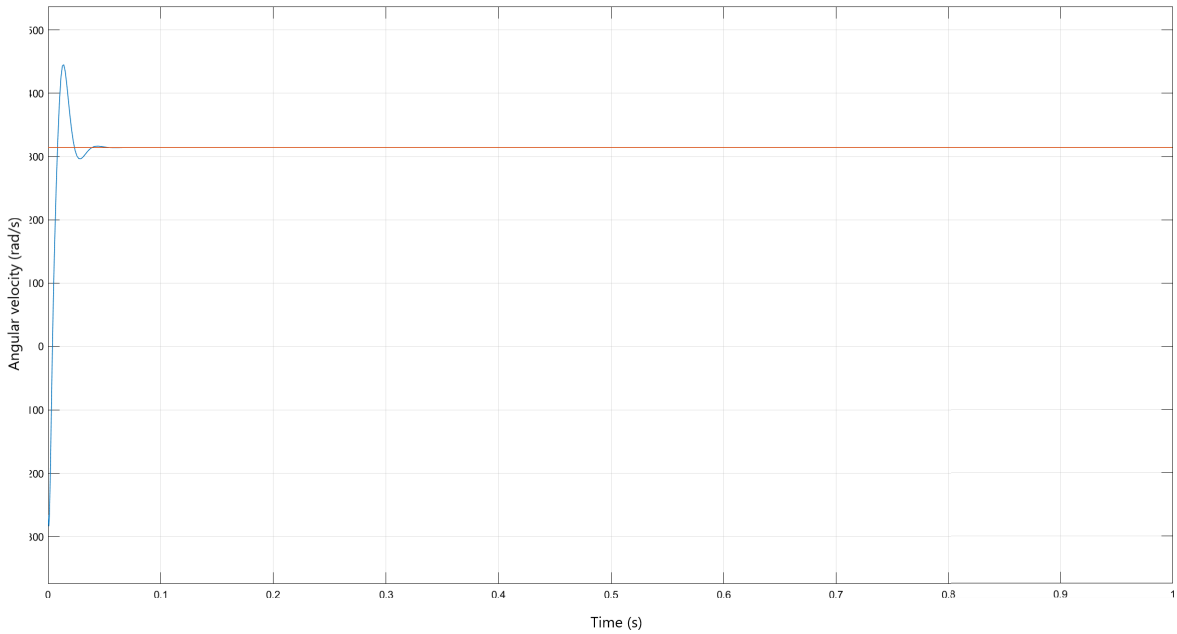

Figure 35: angular velocity of the grid (blue) and its reference (red).

7.1.2 Reference computation

The reference currents in the qd0 reference frame can be calculated using the active and reactive power references.
The equations derived from the Instantaneous Power Theory (IPT) are as follow:

$$P^* = 1,5(v_{zq} i_q^* + v_{zd} i_d^*) \tag{7.5}$$

$$Q^* = 1,5(v_{zq} i_d^* - v_{zd} i_q^*) \tag{7.6}$$

Where v_{zq} is the q-axis grid voltage.

Rearranging these equations, the current variables can be isolated. From the PLL it is known that $v_{zd} = 0$ as it was set like that, therefore the equations are:

$$i_q^* = \frac{2P^*}{3v_{zq}} \tag{7.7}$$

$$i_d^* = \frac{2Q^*}{3v_{zq}} \tag{7.8}$$

Both power reference values will be predetermined for this model, although the active power reference will be obtained from the voltage loop when the PV system is integrated.

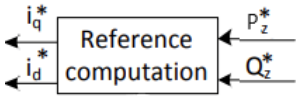

Figure 36: Working method of the reference computation.

7.1.3 Current loop

The output of the previous section, i_q^* and i_d^*, will be used for this loop.
The main objective of the current loop is determining the voltages that the VSC needs to apply AC side. This will be achieved by applying a PI controller to the currents in order to ensure they follow the references deduced previously using the IPT:

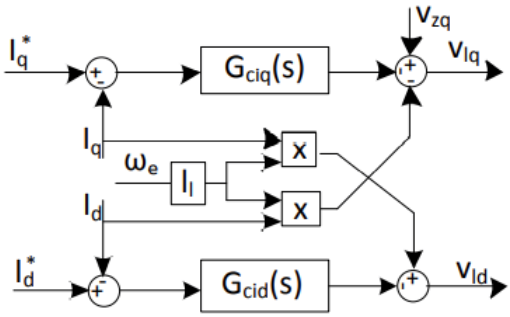

Figure 37: Scheme of the current loop control with its controllers G_{ciq} and G_{cid}.

In section 7.1.1 it was concluded that $v_{zd} = 0$ and thus, equation 5.5 can be rewritten as:

$$\begin{bmatrix} v_{zq} \\ 0 \end{bmatrix} - \begin{bmatrix} v_{lq} \\ v_{ld} \end{bmatrix} = \begin{bmatrix} r_l & l_l\omega_e \\ -l_l\omega_e & r_l \end{bmatrix} \begin{bmatrix} i_q \\ i_d \end{bmatrix} + \begin{bmatrix} l_l & 0 \\ 0 & l_l \end{bmatrix} + \frac{d}{dt} \begin{bmatrix} i_q \\ i_d \end{bmatrix} \tag{7.9}$$

Where it can be seen there is an apparent coupling between the q and d components of both voltages and currents. Therefore, to properly control the current components, decoupling the variables and applying separate controllers.
Otherwise, a two-dimensional controller could be implemented, although the first option is more straightforward and viable for this study.

The decoupling process yields the following equation:

$$\begin{bmatrix} v_{lq} \\ v_{ld} \end{bmatrix} = \begin{bmatrix} -\hat{v}_{lq} + v_{zq} - l_l\omega_e i_d \\ -\hat{v}_{ld} + l_l\omega_e i_q \end{bmatrix} \tag{7.10}$$

Commbining equations 7.9 and 7.10:

$$\begin{bmatrix} \hat{v}_{lq} \\ \hat{v}_{ld} \end{bmatrix} = \begin{bmatrix} r_l & 0 \\ 0 & r_l \end{bmatrix} \begin{bmatrix} i_q \\ i_d \end{bmatrix} + \begin{bmatrix} l_l & 0 \\ 0 & l_l \end{bmatrix} + \frac{d}{dt} \begin{bmatrix} i_q \\ i_d \end{bmatrix} \tag{7.11}$$

Which, transforming into the Laplace domain:

$$\frac{\hat{v}_{lq}(s)}{i_q(s)} = \frac{1}{l_l s + r_l} \tag{7.12}$$

$$\frac{\hat{v}_{ld}(s)}{i_d(s)} = \frac{1}{l_l s + r_l} \tag{7.13}$$

The controller itself will be designed using the Internal Model Control method (IMC), which stipulates a novel procedure compared to the classic control structure (Figure 38) [16]:

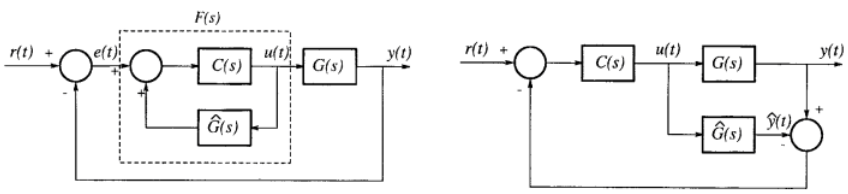

Figure 38: Control schemes of traditional controllers (left) and IMC (right). [16]

IMC was introduced initially in the chemical engineering field as a robust control method. Due to its simplicity, it has been widely accepted, despite having various drawbacks. The main ones are their susceptibility to model errors and the need for a stable system in an open-loop to avoid excessive complexity.

The equations that govern this method and will ultimately lead to the deduction of the proportional and integral parameters are as follows:

$$\hat{G}(s) = \frac{1}{l_l s + r_l} \tag{7.14}$$

$$C(s) = \hat{G}^{-1}(s) \cdot G_f = \frac{l_l s + r_l}{\tau_c s + 1} \tag{7.15}$$

Where G_f is the low-pass filter used and τ_c is the current loop time constant.

The method continues:

$$\hat{G}_c(s) = \frac{C(s)}{1 - C(s)\hat{G}(s)} \tag{7.16}$$

$$\hat{G}_c(s) = G_{ciq} = G_{cid} = K_{pc} + K_{ic}/s \tag{7.17}$$

Finally, combining these last two equations yields the control parameters' expressions:

$$K_{pc} + K_{ic}/s = \frac{l_l}{\tau_c} + \frac{r_l}{\tau_c s} \tag{7.18}$$

$$K_{pc} = l_l/\tau_c \tag{7.19}$$

$$K_{ic} = r_l/\tau_c \tag{7.20}$$

The tuning of the time constant has been carried out considering the physical restrictions of the system. Therefore, it is set to be ten times faster than the converter's switching frequency.

Overall, the control process can be simulated with the use of Simulink, including all the different processes, as:

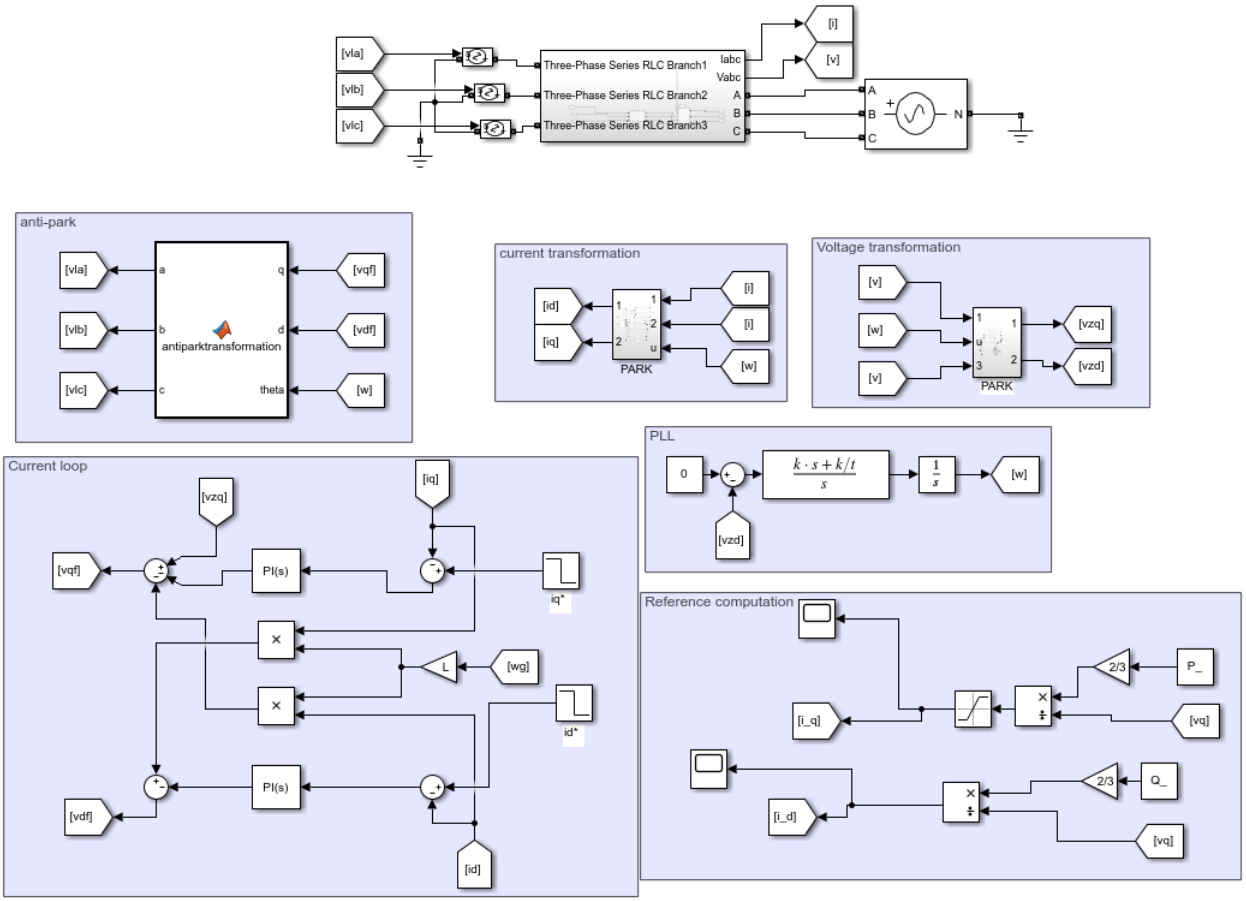

Figure 39: General Simulink model containing all the control systems.

To validate the control model exposed in this section, a series of graphics have been plotted in order to compare both current signals: reference and real. As it can be observed in Figures 40 and 41, the current displays a controlled first-order response in line with the PI controller implemented:

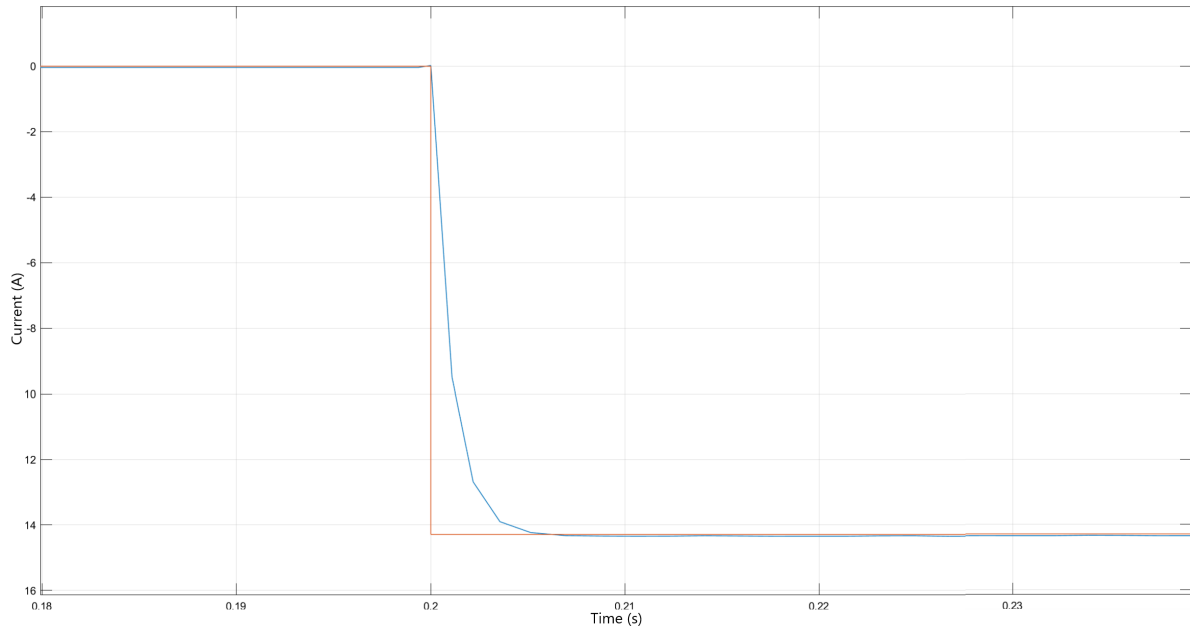

Figure 40: Simulation of i_q (blue) and the reference i_q^* (red).

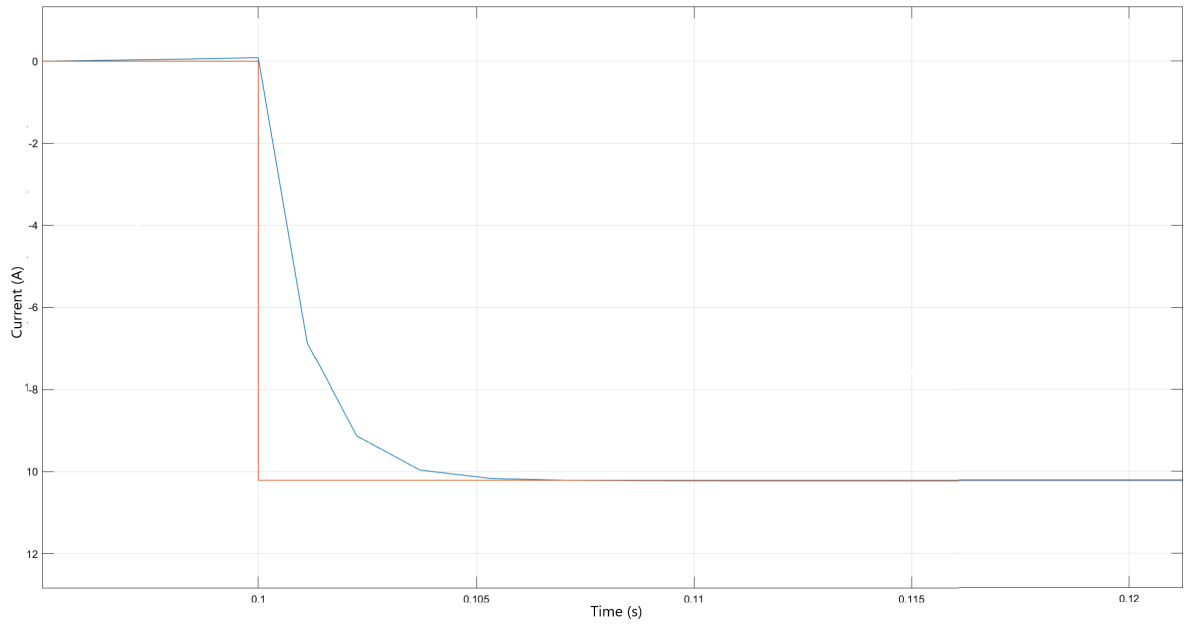

Figure 41: Simulation of i_d (blue) and the reference i_d^* (red).

7.2 Photovoltaic source control

The inclusion of a PV system adds complexity to the control system, especially on the DC side of the VSC. However, systems such as the PLL are not affected while another current loop is integrated to regulate the voltage on the PV side.

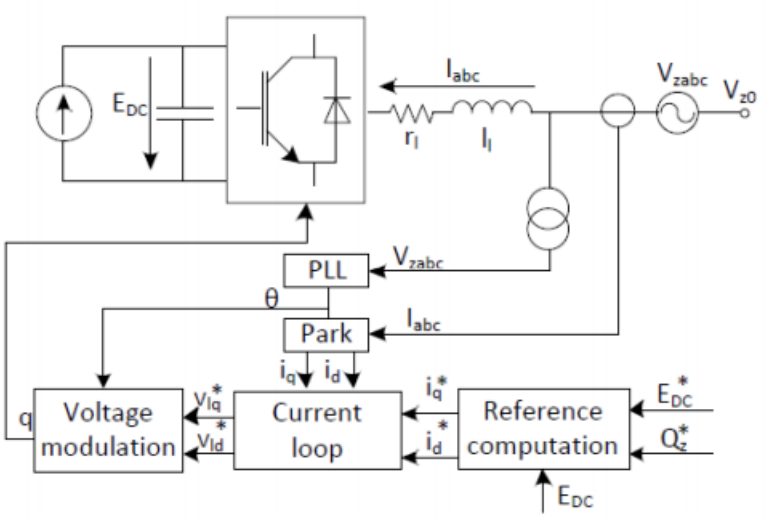

Figure 42: General control scheme for the PV source model. [20]

7.2.1 DC Voltage loop

The DC bus seen in the PV system (Figure 42) needs modulation, reason why the Voltage loop is included. Moreover, it ensures an active power balance between AC and DC sides of the converter.
This power balance between the AC and DC side will be achieved by controlling the current of the VSC on the DC side:

$$I_{DCl} = P_{AC}/E_{DC} \tag{7.21}$$

A representation of the system can be observed in Figure 43:

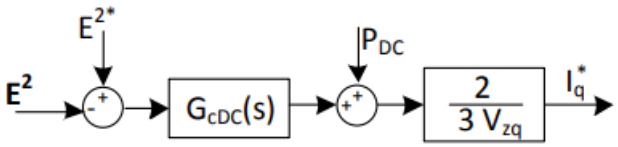

Figure 43: Voltage loop control system representation. [20]

Because the output of the Voltage Loop is the current reference in the q-axis, it makes use of the IPT. First, however, the d-axis component will be derived in the same way as described in section 7.1.2.

The control variable used is $W = E^2$ in a feed-forward scheme, on account of W being directly proportional to the energy stored in the capacitor. In turn, the power reference can be calculated as:

$$P^* = P_c + P_{DC} \tag{7.22}$$

$$P_c = \frac{1}{2} sCW(s) \tag{7.23}$$

Where:
P_{DC} = power through the capacitor.
C= capacitor's capacitance.

A PI controller will be used:

$$G_{cDC} = K_{pDC} + \frac{K_{iDC}}{s} \tag{7.24}$$

Which computed into the closed-loop transfer function:

$$\frac{W(s)}{W^*(s)} = \frac{sK_{pD}C + K_{iDC}}{0{,}5s^2C + sK_{pDC} + K_{iDC}} \tag{7.25}$$

Similar to the form:

$$\frac{W(s)}{W^*(s)} = \frac{2s\xi\omega_n + \omega_n^2}{s^2 + 2s\xi_{DC}\omega_n + \omega_n^2} \tag{7.26}$$

Therefore, both the proportional and integral components of the control can be calculated:

$$K_{pDC} = C\xi_{DC}\omega_n \tag{7.27}$$

$$K_{iDC} = \frac{C\omega_n^2}{2} \tag{7.28}$$

Similarly to other sections, the model can be validated through simulation in Matlab/Simulink. In Figure 46, the DC voltage along the capacitor follows the reference, although with some adjustment time each time the reference varies.

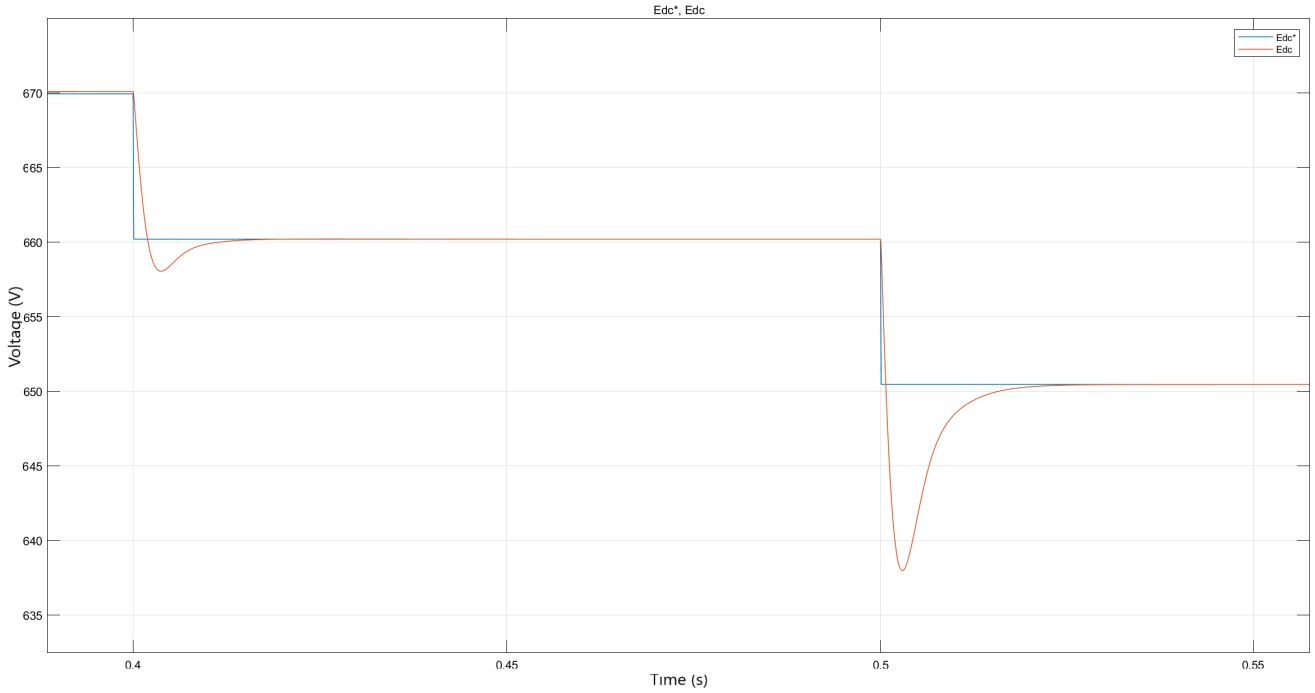

Figure 44: Simulation of E_{DC} (red) and E^*_{DC} (blue).

Finally, the variables seen in this section are given the following values:

C	1020 μF
Damping ratio ξ_{DC}	0,707
angular velocity ω_n	418,88 (rad/s)
Kp_{DC}	0,3021
Ki_{DC}	89,46

Table 5: Parameters for the DC voltage loop control

7.2.2 Current loop

The same current loop seen in section 7.1.3 is the same one applied for this model, with the only difference being the origin of the current references.
As mentioned before, the q-axis component is derived from the voltage loop while the d-axis comes from the reference computation seen in the battery model:

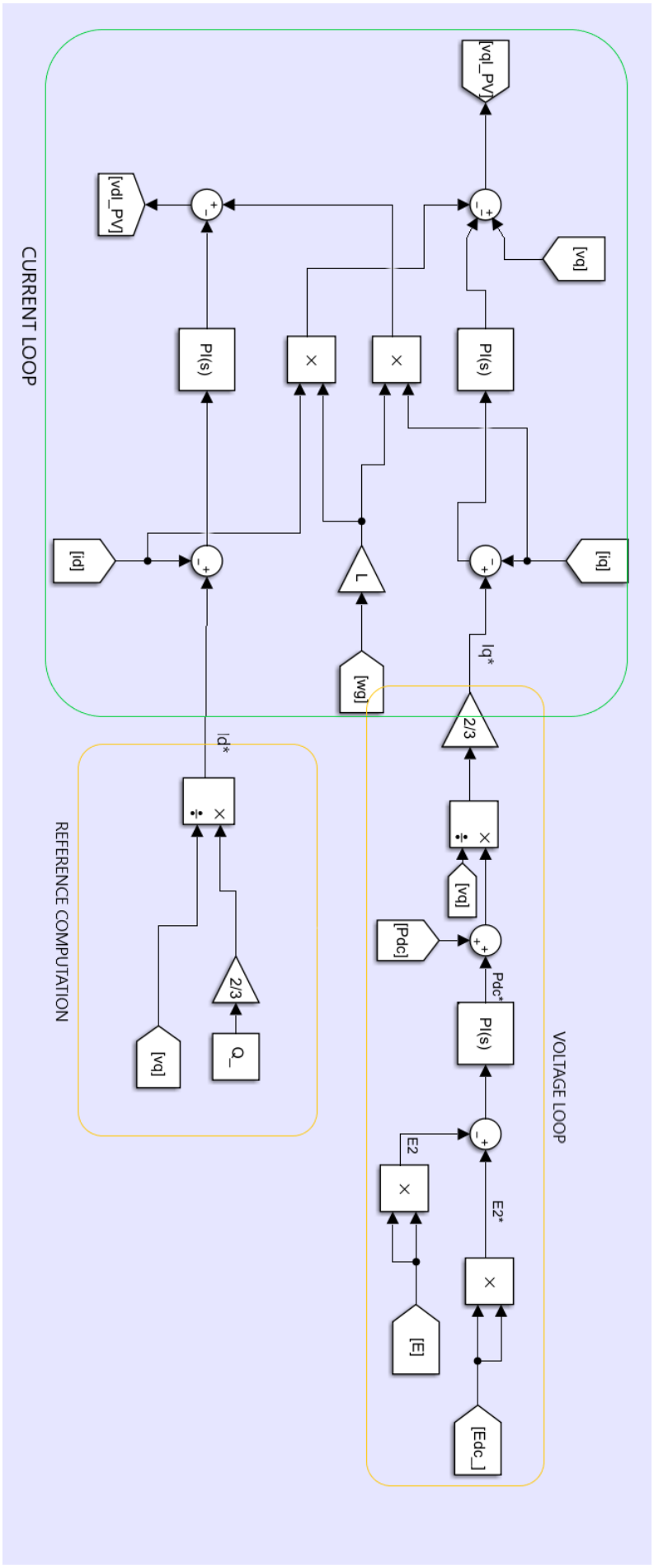

Figure 45: Simulink model of the control systems involved in the PV source model.

Equally to the current loop in the battery model, Figure 46 is a validation of the control method described:

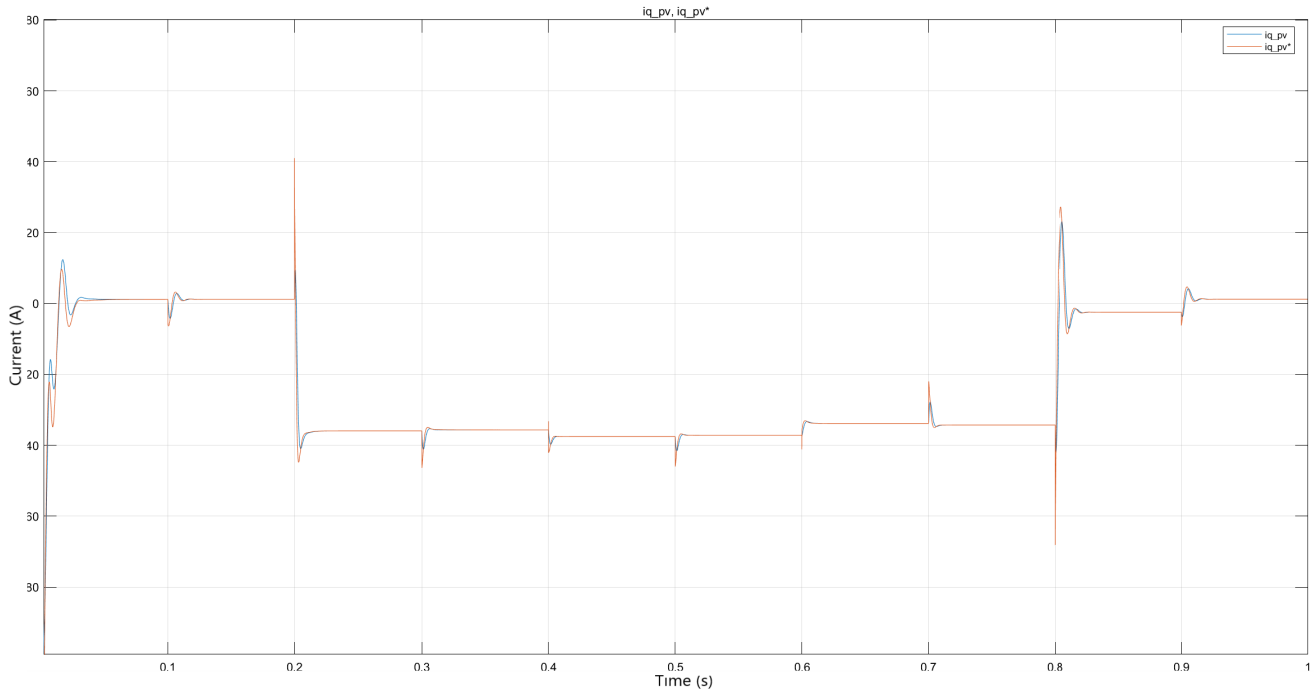

Figure 46: current i_{qPV} (blue) and reference i^*_{qPV} (red).

7.2.3 MPPT algorithms for PV systems

In section 6.1 the behaviour of the PV array was seen alongside its performance.
The main objective when installing a PV system is maximizing the efficiency, and therefore its power output. To achieve this, an MPPT system was implemented, which ensures the PV modules operate at the voltage that translates to peak power output.
The output of said system will be the DC voltage reference, which will be used in the voltage loop seen in section 7.2.1.

All PV panels demonstrate the same behaviour in terms of their I-V curve, where there's a maximum voltage V_{oc} and a maximum current I_{sc} at which it can operate but neither of those points yield any power.
Therefore, the maximum power drawn from any PV module can be found at what is called the 'knee' of the I-V curve.

There are many MPPT algorithms to be considered in order to ensure they work at this operating point, but the one used will be the Fractional Open-Circuit Voltage (FOCV), which postulates that a linear dependency can be observed between the Maximum Power Point (MPP) and V_{oc}:

$$V_{mpp} = k \cdot V_{oc} \tag{7.29}$$

Where k is a constant that is contingent upon the type of the PV module and its configuration.
FOCV is a robust and simple method that does not require a micro-controller, which is why it has been implemented in this model. However, it presents some drawbacks: there's some temporary power loss as well as being a crude approximation.

In section 6.1.1, the parameters of the PV array were laid out, which can now be used to calculate the parameter k:

$$k = V_{mpp}/V_{oc} = 0,814 \tag{7.30}$$

The PV model can be sketched with the inclusion of the MPPT algorithm:

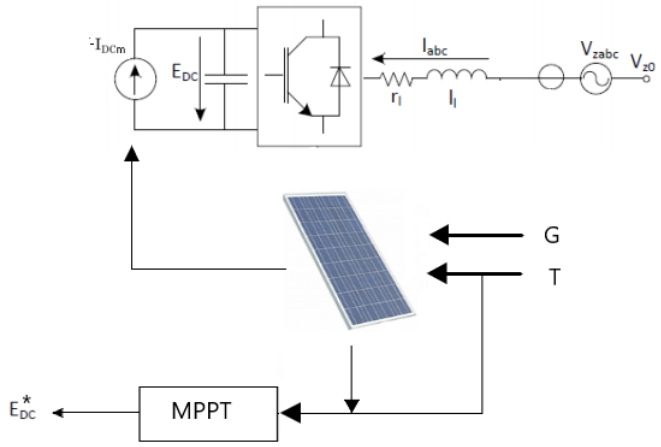

Figure 47: MPPT operation scheme integrated into the MG.

Finally, because the open-circuit voltage is dependent on the Temperature of the PV array, a function needs to be implemented in the model able to output the correct value. This function will be derived from the fact that V_{oc} is found at the point where the current flowing through the module is null:

$$0 = I_L - I_o \cdot (exp\frac{qV_{oc}}{nKT} - 1) - \frac{V_{oc}}{R_s h} \tag{7.31}$$

$$V_{oc} = \frac{nKT}{q} ln(1 + \frac{I_L}{I_0}) \tag{7.33}$$

Where the current flowing through the shunt resistance has been neglected for simplicity purpose.

Otherwise, the V_{oc} temperature coefficient (β) could be used for the same purpose:

$$V_{oc} = V_{ocT1}(1 + \beta(T - T_1)) \tag{7.34}$$

7.3 Grid power control

The last control mechanism designed for this project is an outer layer which establishes the active and reactive power injected or fed by the main grid.
The objective of such task is to avoid calculating and testing different values for the other elements and assessing how in turn the main grid reacts. Bypassing this process aids in the simplification of the study of the overall behaviour of the MG, which will be carried out in section 8.3.

A basic schematic of the inner workings of the control method used can be observed in Figure 48. From this starting point, the Simulink model can be built upon this basic structure:

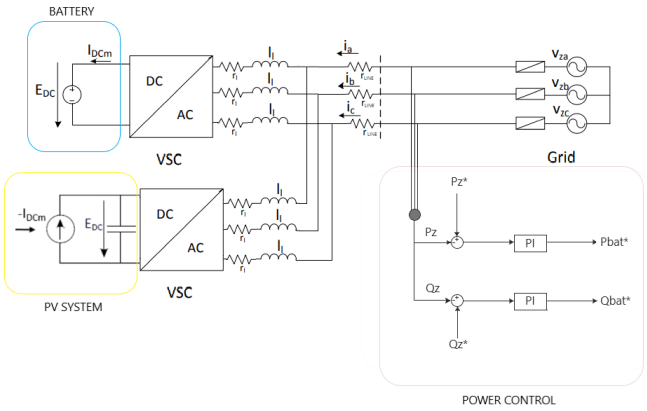

Figure 48: General scheme of the power control.

The implementation of this controller, which will be the same for both active and reactive power, is based on the IMC method, same one used for the current loop in sections 7.1.3 and 7.2.2.

Normally, in order to design a PI controller, both the proportional and integral components need to be computed from the system's plant and the controller's expression in the Laplace domain. However, given that the plant is the combination of multiple processes that take place around the model, such as the current and different impedances,

the final expression would be too complex to work with.
To work around this obstacle, the whole system has been simplified into a first order system with a determined time constant, which in this case is the current loop's time constant.

Having established this, the procedure of determining both of the parameters that define the controller becomes very simple. The same steps as in section 7.1.3 have been taken.

Starting from the simplified first order expression:

$$\hat{G}(s) = \frac{1}{\tau_c s + 1} \tag{7.35}$$

The controller can be expressed as:

$$G_f(s) = \frac{1}{\tau_p s + 1} \tag{7.36}$$

Where τ_p is the time constant for the power control loop, which has been set to 0,1 ms.

The IMC method continues as follows:

$$C(s) = \hat{G}^{-1}(s) \cdot G_f(s) = \frac{\tau_c s + 1}{\tau_p s + 1} \tag{7.37}$$

$$\hat{G}_c(s) = \frac{C(s)}{1 - C(s)\hat{G}(s)} \tag{7.38}$$

$$\hat{G}_c(s) = K_{pp} + K_{ip}/s \tag{7.39}$$

Finally, combining equations 7.38 and 7.39:

$$K_{pp} = \tau_c/\tau_p = 10 \tag{7.40}$$

$$K_{ip} = 1/\tau_p = 10000 \tag{7.41}$$

The response of this system is that of a second-order, resulting from the combination of two first-order systems as deduced in equation 7.38.
This can be demonstrated via simulation, using the same software and methods used in all previous sections.

Figure 49 demonstrates a random simulation in order to show the response of the system according to a varying reference:

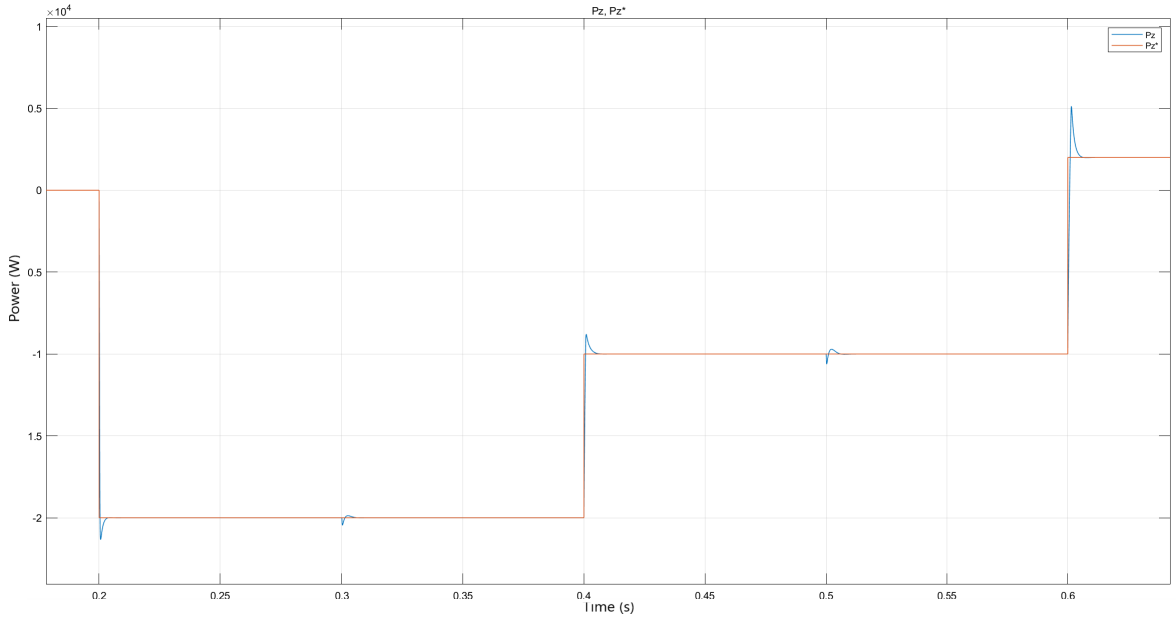

Figure 49: Response of the active power (P_z) vs the reference (P_z^*).

It is safe to say that the controller fulfils its main objective of allowing to assign a reference power point for the system to follow and works properly, as shown by Figure 49.

8 Simulations

This chapter will attempt to validate all the modelling done in previous sections by simulating in Matlab and Simulink. The behaviour of all the elements implicated will be studied, those being the VSC, the DC energy sources and the main grid.
The main focus of this process will be the power exchange between all these components and how they interact to comply with all the energy requirements.

As has been previously mentioned, the MG can operate drawing energy from the main grid, due to an insufficient injection by the energy sources, or feeding to the main grid when an excess of energy occurs.
Both of these cases will be thoroughly studied in this section.

All the simulations have been carried out with a time of 1 second in order to lower the time it takes to run all the software. Hence, every time-dependable variable will be adjusted accordingly, such as the temperature at which the PV modules are operating and the irradiance they receive.

The final model used for this section will be the combination from both models, battery plus PV system, explained in section 5 and 6 respectively. This process will be achieved by the use of a VSC for each of these elements.

One last thing to consider are the line losses, which will be determined in function of the maximum current flowing through the electrical cables made of copper according to the AWG standards.
Line losses, however, are not a feature of the VSC plus battery model or PV system, but instead of the MG as a whole, meaning that they will be considered only once.

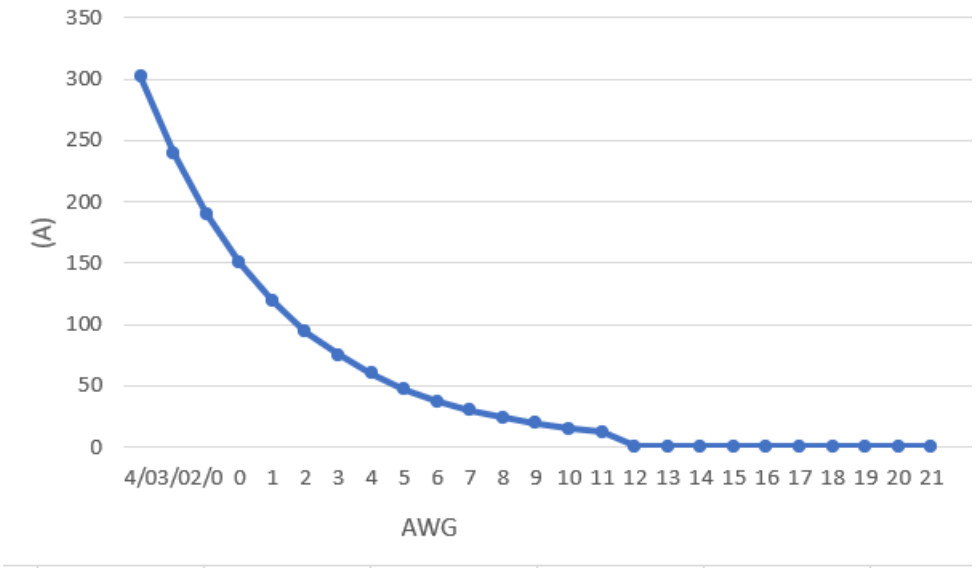

Figure 50: Standardized copper wire sizing (AWG) and its maximum current.

In terms of modelling, they will be inserted between the VSC and main grid as a resistance r_{LINE}(Figure 51).

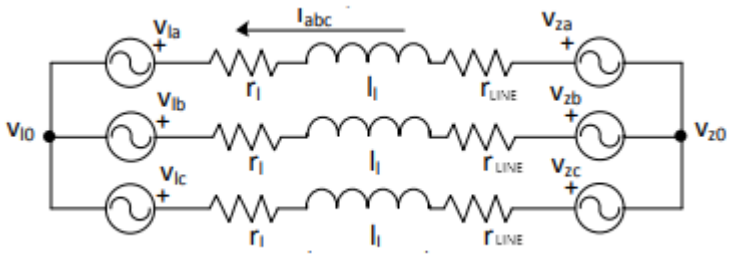

Figure 51: Representation of the MG's AC side with the addition of line losses.

8.1 Parameters

The first step towards simulating the models is establishing all the necessary variables. Starting with the parameters of the grid, the following table contains all the relevant information regarding its specificacions:

r_l	0,5 Ω
l_l	0,0054 F
r_{LINE}	0,0815 Ω

Table 6: Impedance paramaters and respective values

The value of the line losses r_{LINE} has been deduced from the American Wire Gauges (AWG) standards, which establishes the size of the wire needed for each maximum current permitted for power transmission (Figure 50).

Through a multitude of simulations and a safety coefficient of 2, the copper cable AWG 4 has been designated for this project. Therefore, the maximum amperage allowed is 60A (as seen in Figure 50), with a diameter size of 5,2mm.

The resistance this wire presents is $0{,}815(\Omega/\mathrm{km})$, which translated to a 100m of distance yields the value observed in Table.

Moving on, the next element integrated in the simulation that needs parameterizing is the load.

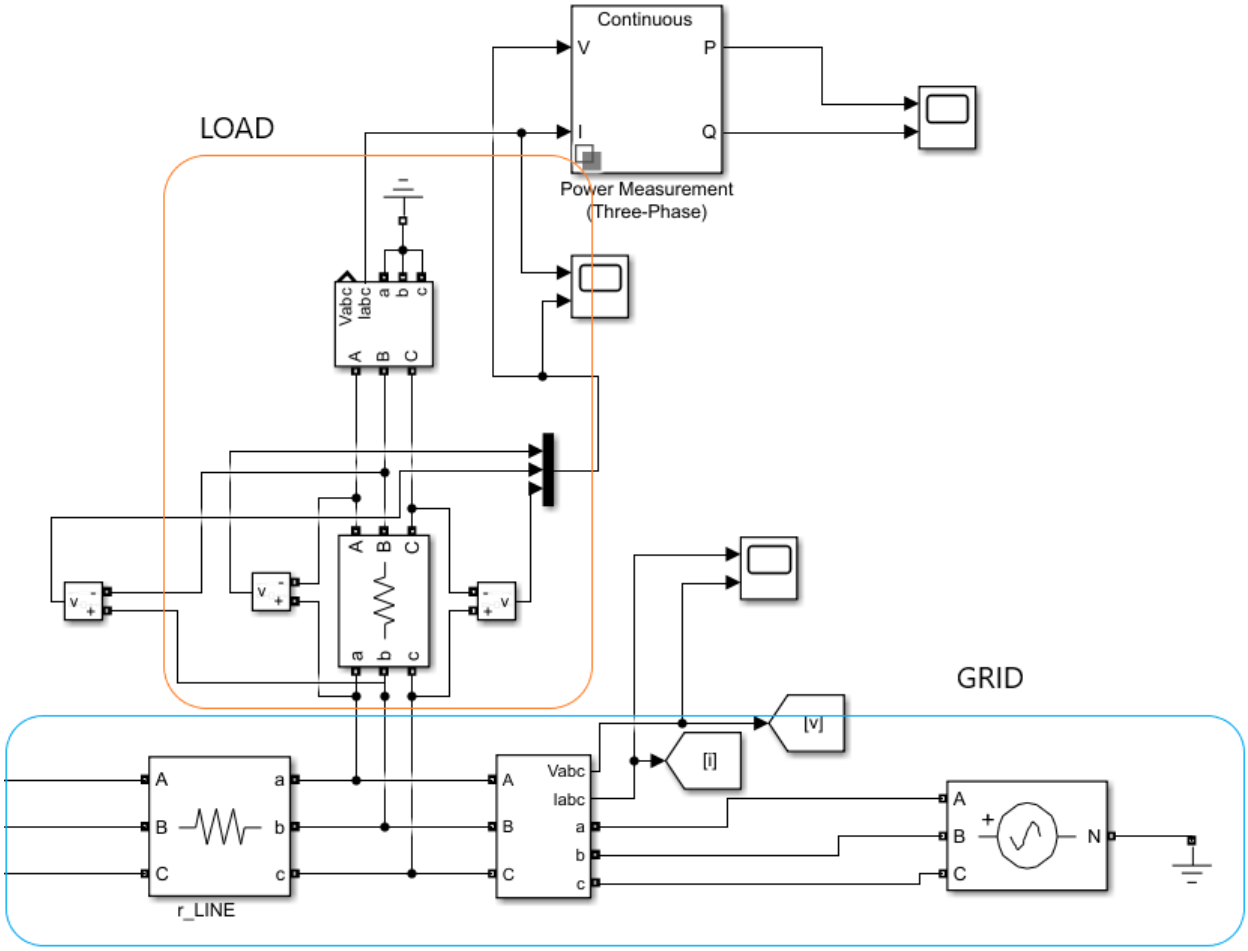

Figure 52: Simulink scheme integrating an AC load into the grid.

In Figure 52 it can be observed how the load has been modelled as a parallel 3-phase resistance to the grid (r_{LOAD}). Thus, the power flowing through the load will be active power in its totality.

Part of the power generated by the renewable source is going to be utilized by an AC load simulating an apartment building. Taking into account the fact that on average an apartment consumes 4 KW approximately, the AC load will be rated at 30 KW with (r_{LOAD}) being 8Ω:

$$P_{LOAD} = 3\frac{(V_{lin}/\sqrt{3})^2}{r_{LOAD}} \tag{8.1}$$

$$P_{LOAD} = 3\frac{(V_{lin}/\sqrt{3})^2}{8} = 30KW \tag{8.2}$$

8.2 Photovoltaic source results

This chapter will treat all the simulations and results relating to the PV system.

Firstly, as it was modelled in chapter 6, the PV array needs 2 input signals: operating temperature and irradiance gathered by the PV modules.
Because the simulation time is 1 second, both of these signals need to be proportionally adjusted.

The data used for the irradiance will be gathered from the city of Barcelona [17], and approximated to the values seen in Figure 51:

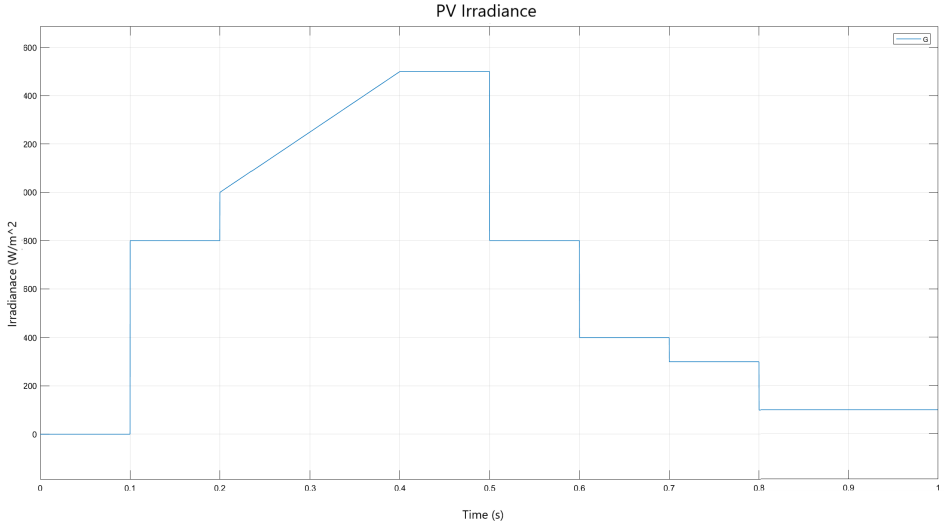

Figure 53: Irradiance values in Barcelona during the day.

On the other hand, the temperature values have been approximated to an average day in May in the same city:

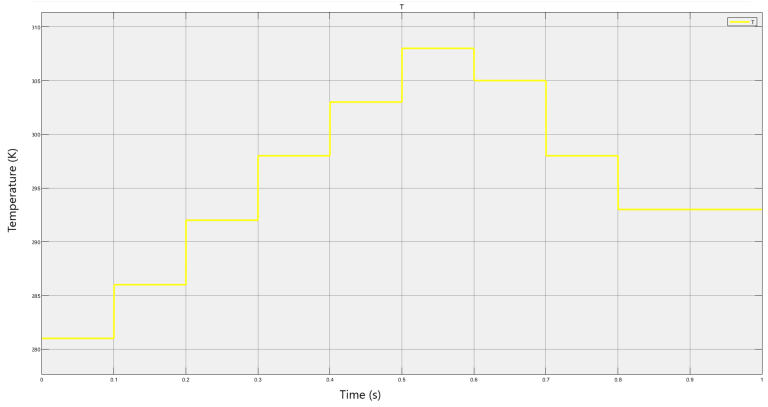

Figure 54: Temperature input used for simulations in Simulink.

All relevant outputs resulting from the PV system have been simulated, including both the voltage and current injected into the MG.

First of all, the DC bus voltage has been plotted in Figure 55, where the control mechanism explained in section 7.2.1 can be observed to work to perfection.
Moreover, examining how little deviation there is between the DC voltage and the reference voltage E^*_{DC} it can be concluded that the MPPT algorithm is also functioning as is supposed. The maximum power point at which it can operate is also at the voltage reference.

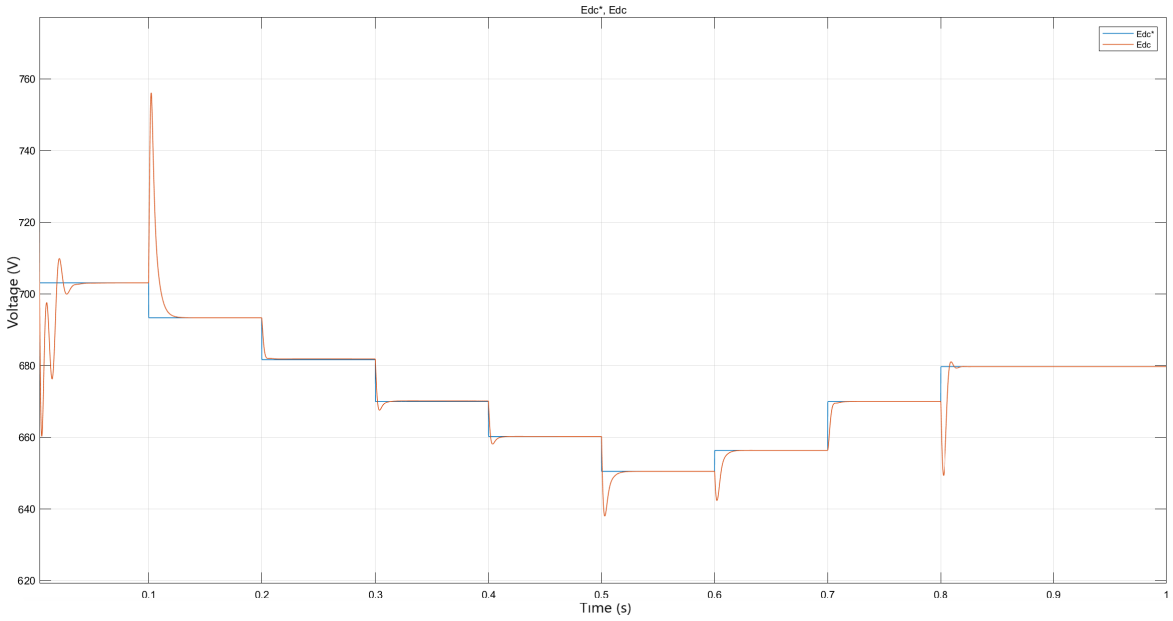

Figure 55: Evolution of the DC bus voltage.

Zooming into this plot, the minimal difference between both signals can be discerned in Figure 56. With a simple calculation it was determined that the deviation is below 0.03%:

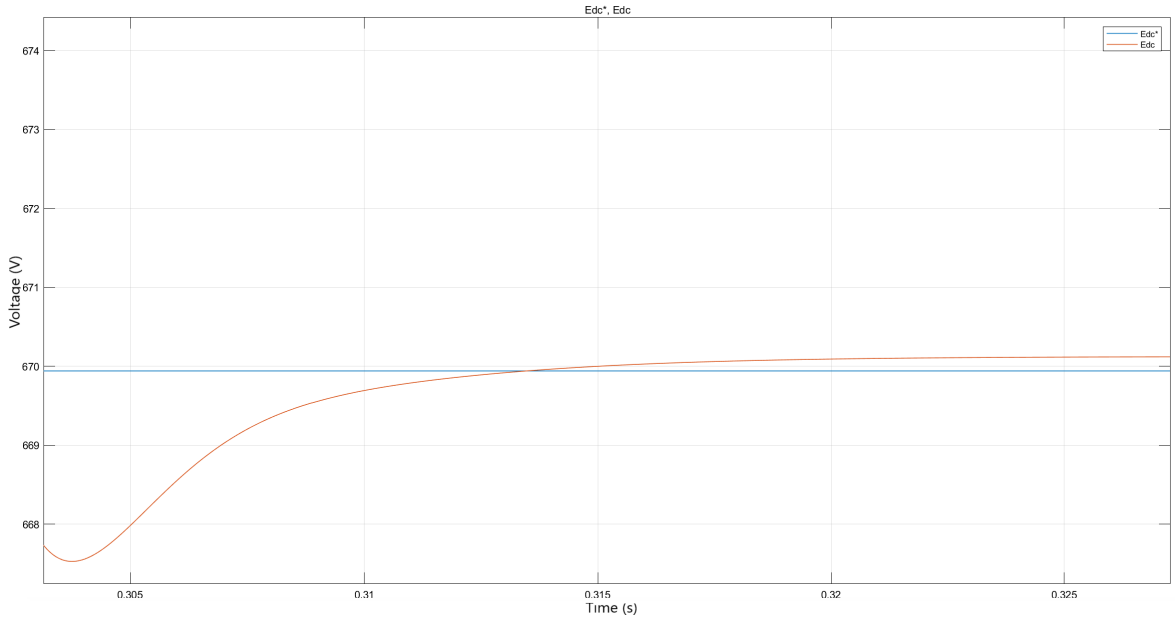

Figure 56: Close up of the PV DC voltage.

On the other hand, the q component of the current generated by the PV system in the qd0 reference frame changes according to the irradiance captured by the PV modules, plotted in Figure 53. It can also be noted that it is symmetrical to the I_{dcm} signal.
The d component however, changes according to the reactive power reference set in the reference computation for the PV system.

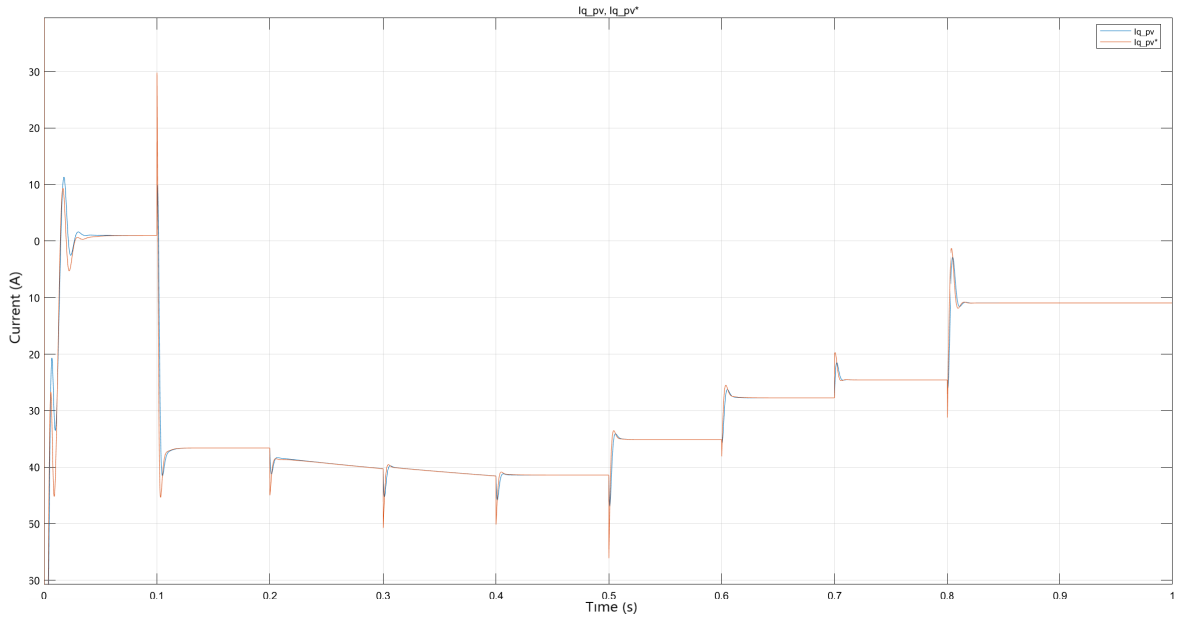

Figure 57: Evolution of I_{qPV} current component vs its reference I^*_{qPV} .

A random simulation has been carried out to showcase the phenomenon described before about the behaviour of I_{dPV} and its correlation to the reference reactive power, seen in Figure 58:

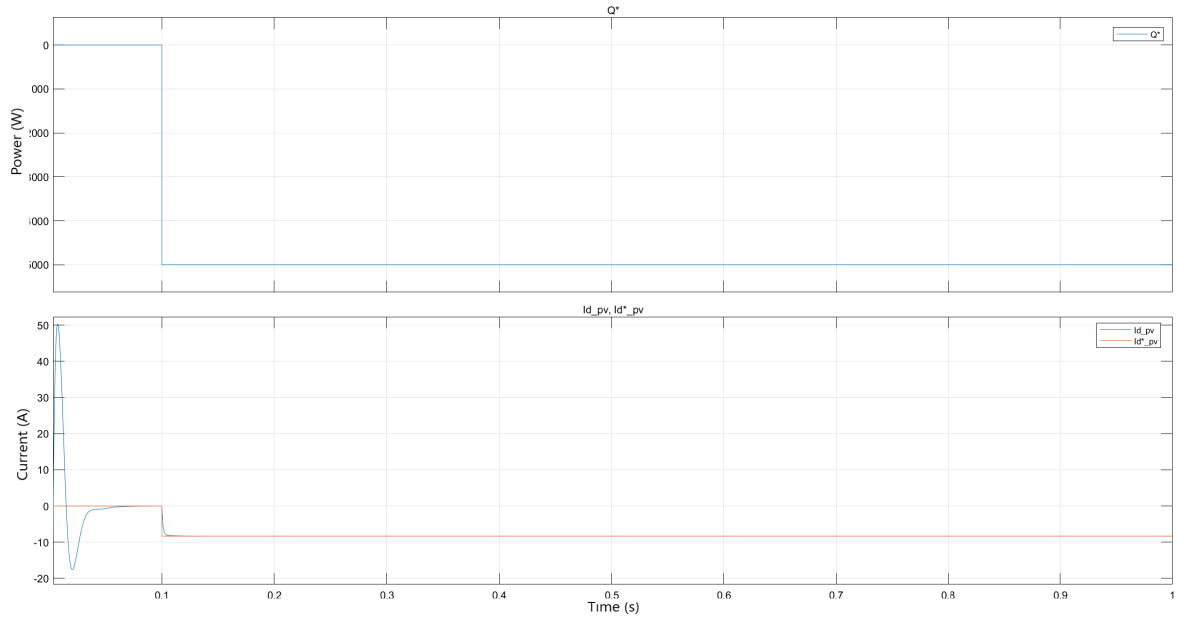

Figure 58: Upper graph shows the evolution of the reactive power reference. Lower graph shows I_{dPV} vs I^{*}_{dPV} .

Finally, the power generated by the PV system can be observed in Figure 59, which will be used in section 8.3 to study the operation of the MG under certain conditions.

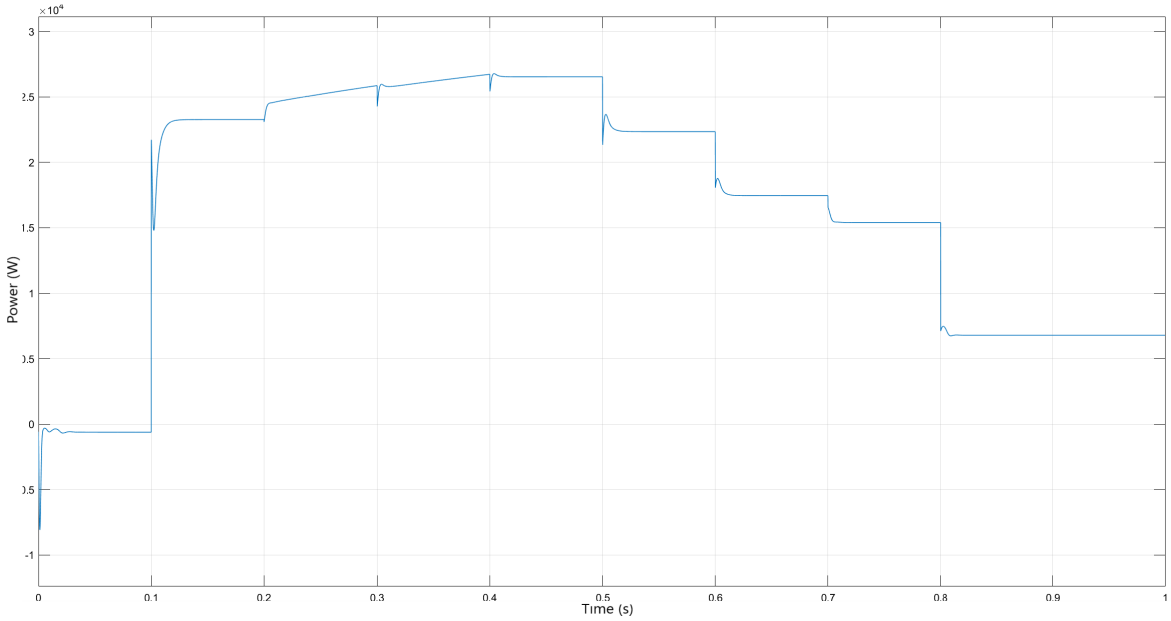

Figure 59: Evolution of the power generated by the PV system .

It can be observed how the power generated fluctuates depending on the irradiation and temperature to a lesser extent. Because the model simulates the passing of a day, at the ends of it the irradiance from the sun is negligible and so, the power generated becomes very low.
On the other hand, when the light of day is at its highest, so is the power output of the PV source.

8.3 General Microgrid operation

The objective for these simulations is to study the behaviour of the whole system depending on whether the MG injects power into the main grid or draws from it.
The control mechanism explained in section () will assist in achieving such goal, as the power that flows through the connecting point between these two elements. This variable can be set to fluctuate from negative to positive values in order to study multiple cases in the same simulation. Figure 53 shows the way it has been adjusted, where P_z^* is the power reference set for the main grid and P_z is the actual response of the system:

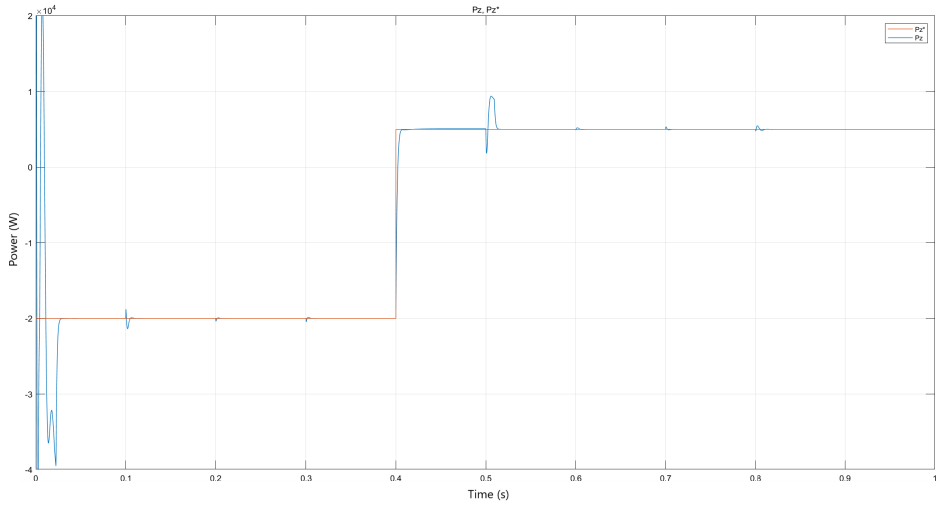

Figure 60: Temperature input used for simulations in Simulink.

Starting from t $= 0s$ to t $= 0.4s$, the MG operates feeding power to the grid as evidentiated by its negative values. However, from t $= 0.4s$ to t $= 1s$ the reverse is true, having positive values.

Having established the overall behaviour of the MG, both the PV and battery systems need detailing. Therefore, all their main characteristics will be plotted and explained, those being their current, voltage and power.

Firstly, the battery's current can be seen in Figure 54, where negative values indicate that the battery is providing power to the MG due to insufficient generation by the PV source. Conversely, positive values of the current designates that the battery is being used to store extra power.
The Park transformation will be used to plot the q-component of the current, given that this is the one that is useful.

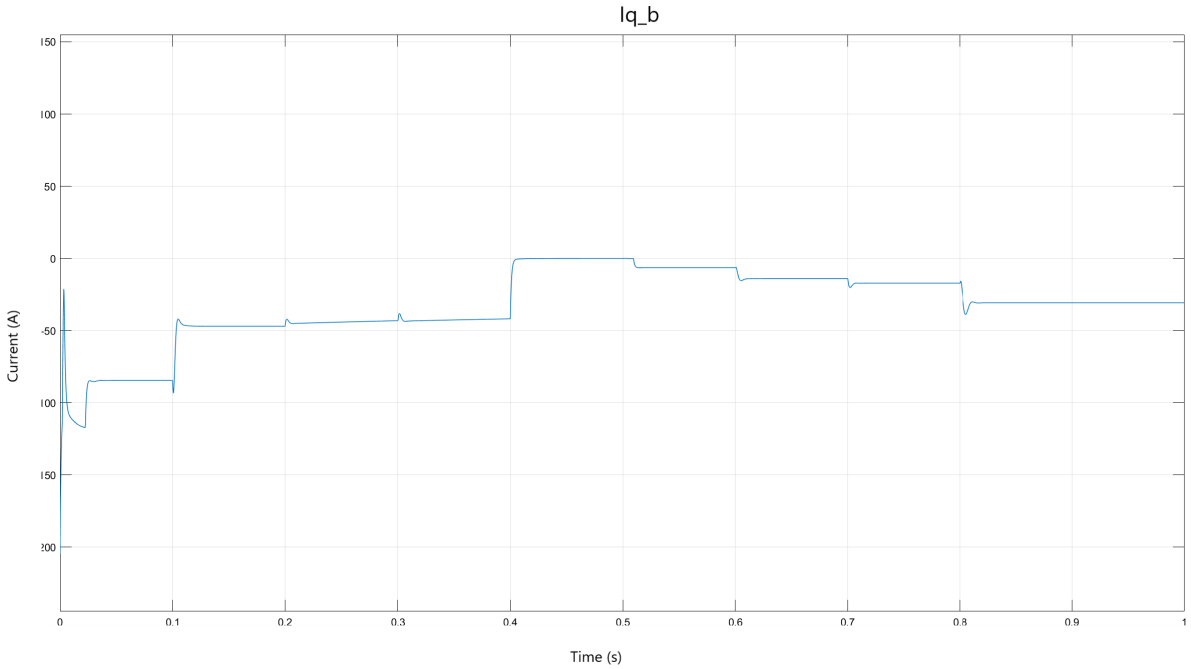

Figure 61: Resulting current for the battery i_{qb} .

The values seen in Figure 54 can be explained by the operating behaviour of the MG. When the main grid is fed at the start of the simulation, the battery needs to inject a substantial amount power to combine with the PV source and achieve the desired power output set at the beginning, resulting in negative current values. Otherwise, when the grid is injecting power the battery is basically at an operating point of neither injecting nor storing energy, as the PV and the main grid are enough to sustain the load. As the simulation continues, emulating the passing of a day, the irradiation from the sun becomes weaker, and so the battery needs to compensate by injecting extra power, increasing the current value along the negative axis of current.

This also explains the active power results, which can be observed in Figure 55. Taking into account that the voltage values for the battery are constant, the current values seen in Figure 54 are proportional to the power values seen in Figure 55:

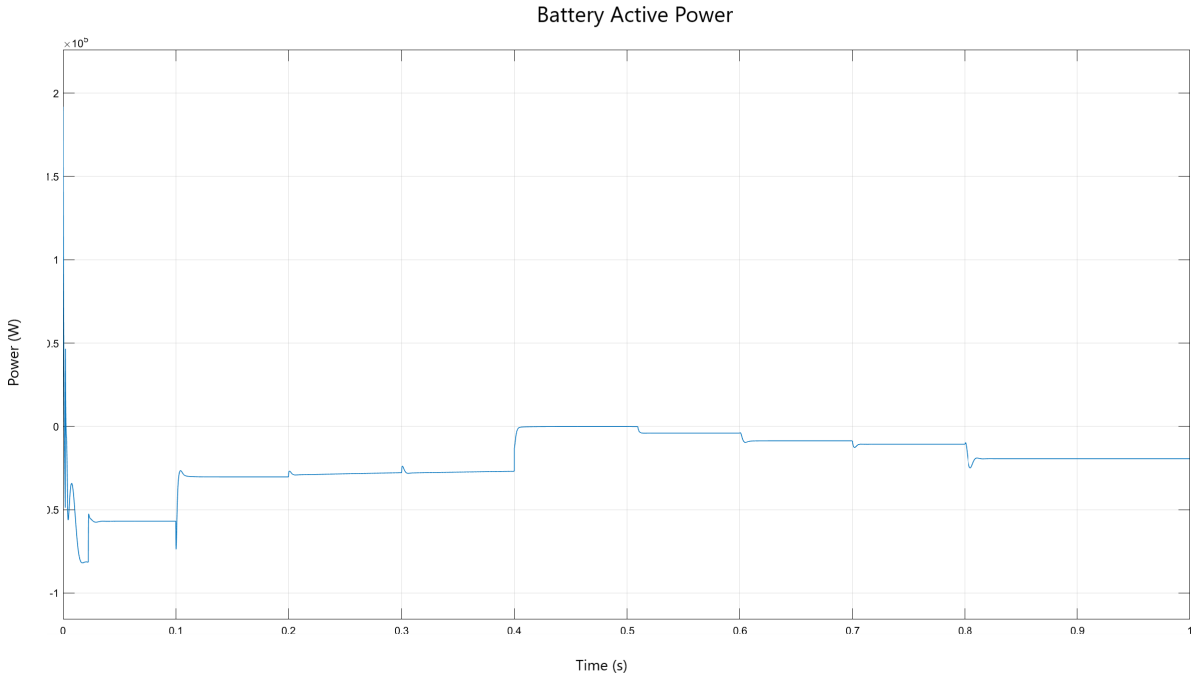

Figure 62: Evolution of the active power in the battery system .

The PV system has already been studied in section 8.2. All the specifications set for the main grid's power does not affect the PV's power output and, thus, all the parameters studied in the previous section prevail for this study case.

Finally, in order to better understand the system in its entirety, all the relevant currents and active powers outputs can be plotted in one single graph and compare them and their evolution.

Figure 56 shows all the q components in the qd0 reference frame of the studied elements' currents:

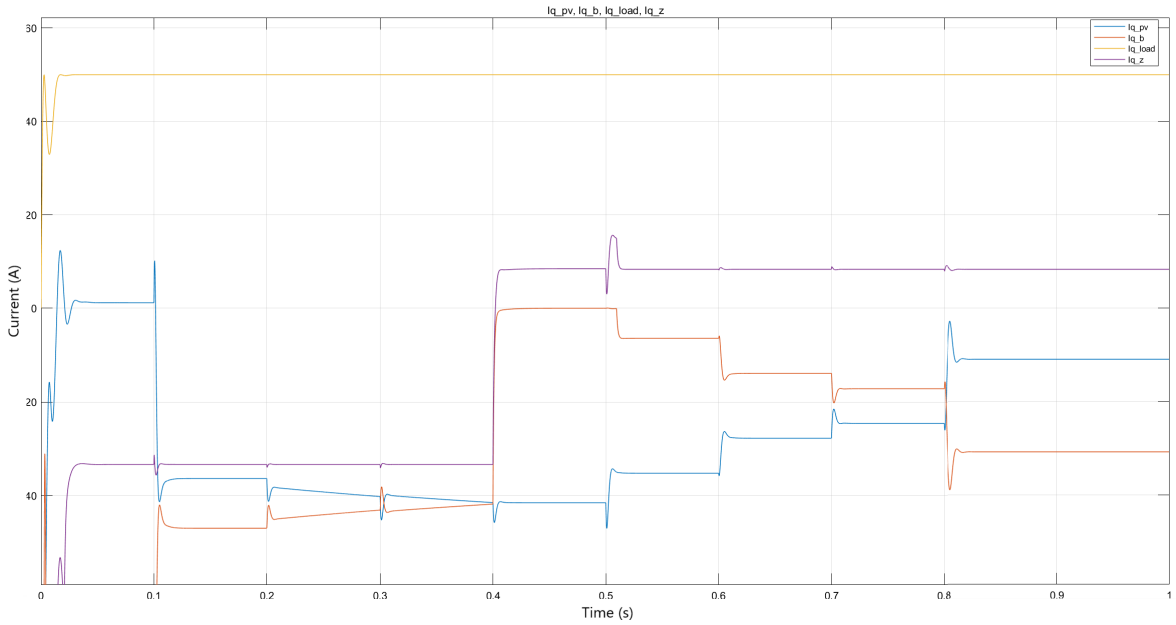

Figure 63: Evolution of all the currents involved .

Where:

i_{qb}= battery current.
i_{qPV}= PV system current.
i_{qLOAD}= Load current.
i_{qz}= grid current.

Additionally, Figure 57 shows the evolution of all the active powers in the same way as Figure 56 does with currents:

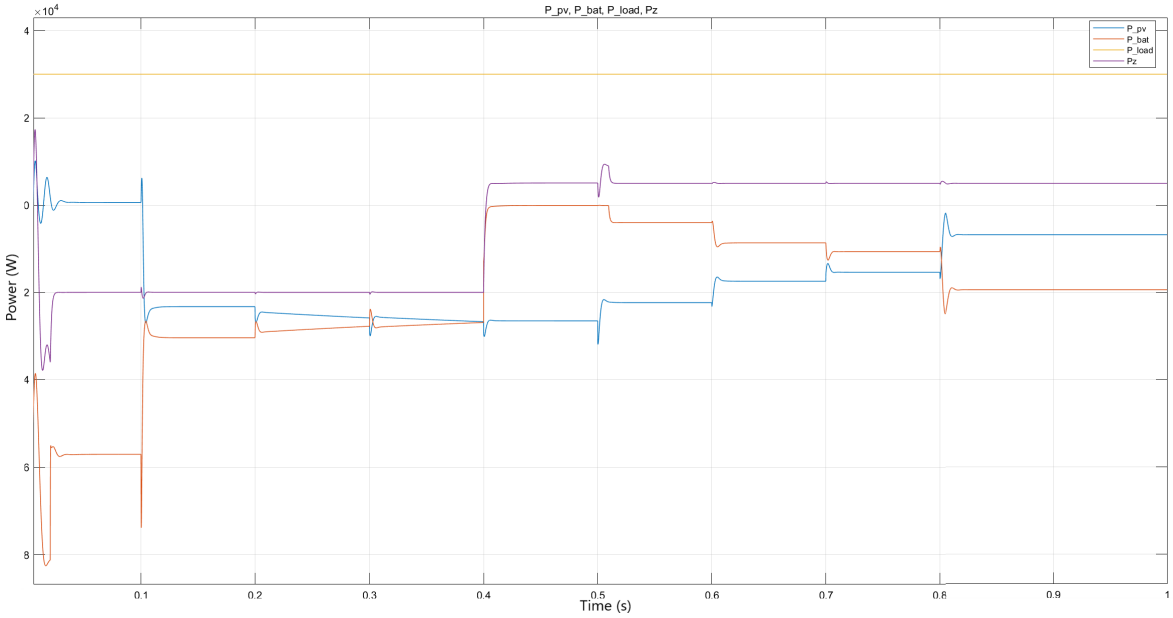

Figure 64: Evolution of all the active powers involved .

These last two plots in conjunction indicate the overall behaviour of the MG. The load is receiving active power coming from the main grid, battery or the PV system depending on the situation, or indeed a combination of some of them. This is reflected in the sign of both current and active power: the model has been built with the positive direction going towards the load.

Furthermore, the mechanisms through which all the active powers are balanced is evident in Figure 57. As mentioned before, in order to satisfy the demands of the load, the battery and grid balance each other as well as the natural variations in the PV system.

9 Economic analysis

This section presents an estimation of the costs realizing this project entails. Due to its complexity and variability, the budget analysis of implementing a MG like the one studied in this project is not feasible.
Therefore, the main focus in this section will be the costs associated with the development and simulation of such study.
These costs can be grouped in two distinct categories: human and material resources.

The bulk of this project is centered around research and development and thus, a majority of the budget will go towards economically compensating the researcher for the amount of time invested in the project.
A rough estimate of the number of hours dedicated can be seen in Table 7, alongside its economic impact.

Item	Price (€/h)	Hours	Total
Research	25	100	2500
Modelling and simulating	25	150	3750
Writing	50	100	2500
Subtotal			8750

Table 7: RD budget and breakdown

On the other hand, the equipment necessary to carry out a project of this caliber entails some additional costs, which are broken down in Table 8:

Item	Price (€)	Units	Total
Laptop	1000	1	1000
Matlab 2020a Software	250	1	250
Accessories & periferals	100		100
Subtotal			1350

Table 8: Equipment budget and breakdown

Thus, the total cost of the project will be:

Item	Total (€)
Human Resources	8750
Material Resources	1350
Subtotal	8750
I.V.A (21%)	2121
Total	12221

Table 9: Total project budget

10 Environmental Impact

During the development of this thesis no polluting equipment has been used other than the equipment laid out in section 9, which means that the environmental footprint is minimal to non-existent. All that needs to be taken into account is the energy consumption of the electronic devices used to realize this project.

The more pressing issue however, is that of the impact implementing some or the totality of the ideas and models explained would have on the environment. Unfortunately, this research falls out of the scope of the project and is therefore not studies.
Nonetheless, the main objective in carrying out and physically implementing these technologies is to reduce the negative environmental impact of traditional grid networks, in favour of a more sustainable solution such as a Microgrid with renewable energy sources.
Furthermore, during this thesis some examples have been discussed about their implementation and impact on their surrounding environment.

11 Conclusions

Throughout this project a model of a MG has been developed, detailing each component within it as well as their behaviour. This would include the PV system, VSC and battery system. Most importantly, their interaction has been examined thoroughly by analyzing their performance separately and collectively via diverse tests and simulations.

Modelling the PV system proved more complex than anticipated, as not only an equivalent electric model representation is required, but also implementing a functioning MPPT algorithm in order to maximize the efficiency of each PV module.
Given the wide array of possibilities in the solar modules field, scrutinizing the parameters of different options proved a significant variance in the observed performance profile, which needed to be taken into account.
On the other hand, multiple options were investigated for the implementation of an MPPT algorithm, even within the same subcategory.

Overall, the renewable source system was successfully implemented into the model, which presents the added to complexity of connecting a DC source to an AC grid.

Accomplishing such task relies on the proper modelling of Voltage Source Converters, whose simplified model has been validated by its efficiency and results. Deriving the equations that govern the behaviour of VSC led to a proper implementation of control systems which allow the user to regulate the characteristics of the model and each element.

Connecting a DC source to the grid was a process also carried out with the aid of VSC in the case of the storage system, or battery to be more precise. Modelling and studying this element, although less complex, is of extreme importance towards fulfilling the objective set out of studying the complete model of a MG.

As has been mentioned before, all simulations performed in this project have been executed using the software Matlab and Simulink tool, alongside multiple extensions of the latter. Due to the great versatility and flexibility they provide, examining a plethora of study cases and operations for each element in the MG, or indeed as a whole, proved to be immensely helpful and insightful. Ultimately, cementing all the different ideas and knowledge was possible in great part because of the nature of simulating and testing, and the insights they provide.
Moreover, this also applies to different projects. Given that most of the elements involved have been studied separately and how easily they can be molded to the researcher's desires, future projects can make use of some ideas and parts discussed in this thesis.

However, being that MG are a vast field of study, research like this can be built upon to investigate further and create new lines of work. Some ideas will be exposed in the next section.

11.1 Future work

Introductory level research such as the one presented can obviously be expanded in a multitude of ways.

First of all, the model representing a VSC is heavily simplified and one line of work could be applying a real model of a VSC to the overall model. Comparing both results could result in some insightful findings as well as validating or disproving the simplified model presented during this project.
Some kind of Pulse Width Modulation would need to take place in order to modulate the converter voltage, which can lead to an interesting area of research in investigating different kinds of Pulse Width Modulation signals.

Heavy focus has been directed at renewable energy sources, even though only one has been studied. Therefore, another possible expansion of this research would be implementing a wind turbine model alongside the presented PV system. Interesting comparisons could arise from their investigation, coupled with a novel control method for wind energy, which differs from the control loops and MPPT algorithm employed for the PV energy source.

Finally, another simplification used in this thesis is that of the battery model. Further research can be directed at implementing a real model of a battery and, as is the case with VSC, compare both models and draw conclusions over the validity of the simplification. A hybrid energy storage system could even be considered as an expansion to the current project with some interesting ramifications.

References

[1] J.M.Guerrero, *PhD course on AC microgrids*, Aalborg Univrsity, 2014

[2] Utah Energy Hub *Connecting Your Solar to the Grid and Export Credit Rates*, https://hub.utahcleanenergy.org/solar-power/for-homes/connect-to-the-grid/

[3] , *A trick to teach you how to judge the IGBT module is good or bad*, Veichi, 2019, https://www.veichi.org/industry-news/a-trick-to-teach-you-how-to-judge-the-igbt-module-is-good-or-bad.html

[4] M.Shahparasti, *Standalone DC/AC converter*, Southern Denmark Univrsity, 2020

[5] *IGCT–integrated gate-commutated thyristors*, Brown University, https://www.brown.edu/Departments/Engineering/Courses/ENGN1931F/ABB_Flyer_IGCT_2015.pdf

[6] B.Jacobson, P.Karlsson, G.Asplund, L.Harnefors, T.Jonsson, *VSC-HVDC Transmission with Cascaded Two-Level Converters* Cigre, 2020

[7] Mika Ikonen, Ossi Laakkonen, Marko Kettunen, *TWO-LEVEL AND THREE-LEVEL CONVERTER COMPARISON IN WIND POWER APPLICATION* , Lappeenranta University of Technology, January 2005

[8] A. Salem, M. A. Abido, *T-Type Multilevel Converter Topologies: A Comprehensive Review*, King Fahd University of Petroleum Minerals, 2018

[9] Salman Hajiaghasia, Ahmad Salemniaa, Mohsen Hamzehb, *Hybrid energy storage system for microgrids applications: A review*, Colleg of Engineering, University of Tehran, 2019

[10] Solar Energy Industries Association *Solar Industry Research Data*, 2020, https://www.seia.org/solar-industry-research-data

[11] Gaëtan Masson, Alice Detollenaere, July Van Wetter, Gaëtan Masson, *Snapshot of Global PV Markets*, International Energy Agency, 2020

[12] IEA (2020), *Renewables 2020*, IEA, Paris, 2020

[13] IDAE *Renewable energies in Spain*, 2017

[14] Gray, J.L., *he Physics of the Solar Cell, in Handbook of Photovoltaic Science and Engineering*, A. Luque, Hegedus, S., Editor. 2011,

[15] J.A. Gow and C.D. Manning, *Development of a photovoltaic array model for use in power-electronics simulation studies*, 1999

[16] Hans-Peter Nee, Lennart Harnefors, *Model-Based Current Control of AC Machines*

Using the Internal Model Control Method, IEEE, 1998

[17] European Comission JRC, *PVGIS*, https://re.jrc.ec.europa.eu/pvg_tools/es/tools.html

[18] Se-Kyo Chung, *A Phase Tracking System for Three Phase Utility Interface Inverters*, IEEE, 2000

[19] R.H.Park, *Two-reaction theory of synchronous machines*, AIEE Transactions, 1929.

[20] EGEA, A., JUNYENT, A., GOMIS, O., *Active and Reactive Power Control of Grid Connected Distributed Generation Systems.*,Green Energy and Technology, 2011.

Appendix A

Park Transformation

The Park transformation is a useful tool when analyzing electrical three-phase systems, as it simplifies oscillating signals.

First introduced by R.H.Park in 1929 [19], this mathematical device can be expressed as the representation of a three-phase vector into a rotating two-axis frame:

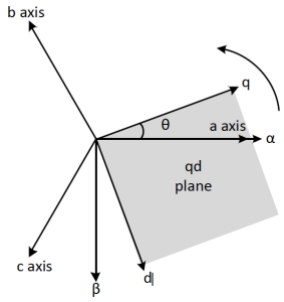

Figure 65: Park transformation representation [20]

$$[x_{qd0}] = T(\theta)[x_{abc}] \tag{A.1}$$

Where x_{abc} is a three-phase vector in the *abc* reference frame, x_{qd0} is the output vector in the *qd0* reference frame and $T(\theta)$ is the Park transformation matrix.
This transformation matrix can be expressed as follows:

$$T(\theta) = \frac{2}{3}\begin{bmatrix} \cos(\theta) & \cos(\theta - \frac{2\pi}{3}) & \cos(\theta + \frac{2\pi}{3}) \\ \sin(\theta) & \sin(\theta - \frac{2\pi}{3}) & \sin(\theta + \frac{2\pi}{3}) \\ \frac{1}{2} & \frac{1}{2} & \frac{1}{2} \end{bmatrix} \tag{A.2}$$

The inverse transformation can also be described similarly, starting from a vector in the *qd0* reference frame and achieving a vector in the *abc* reference frame:

$$T(\theta)^{-1}[x_{qd0}] = [x_{abc}] \tag{A.1}$$

Where:

$$T(\theta)^{-1} = \frac{2}{3}\begin{bmatrix} \cos(\theta) & \sin(\theta) & 1 \\ \cos(\theta - \frac{2\pi}{3}) & \sin(\theta - \frac{2\pi}{3}) & 1 \\ \cos(\theta + \frac{2\pi}{3}) & \sin(\theta + \frac{2\pi}{3}) & 1 \end{bmatrix} \tag{A.2}$$